Supporting Information

Development of a First-in-Class Small Molecule Inhibitor of the C-terminal Hsp90 Dimerization

Sanil Bhatia[1*], Lukas Spanier[2*], David Bickel[2], Niklas Dienstbier[1], Vitalij Woloschin[2], Melina Vogt[1], Henrik Pols,[2] Beate Lungerich,[2] Jens Reiners[3], Narges Aghaallaei[4], Daniela Diedrich[2], Benedikt Frieg[2,5], Julian Schliehe-Diecks[1], Bertan Bopp[6], Franziska Lang[1], Mohan Gopalswamy[2], Jennifer Loschwitz[2], Baubak Bajohgli[4], Julia Skokowa[4], Arndt Borkhardt[1], Julia Hauer[7,8], Finn K. Hansen[9], Sander H.J. Smits[3,10], Joachim Jose[6], Holger Gohlke[2, 5#] and Thomas Kurz[2#]

Affiliations:

1. Department of Pediatric Oncology, Hematology and Clinical Immunology, Medical Faculty, Heinrich Heine University Düsseldorf, Düsseldorf, Germany
2. Institute for Pharmaceutical and Medicinal Chemistry, Heinrich Heine University Düsseldorf, Düsseldorf, Germany
3. Center for Structural Studies, Heinrich Heine University Düsseldorf, Düsseldorf, Germany
4. Department of Hematology, Oncology, Clinical Immunology and Rheumatology, University Hospital Tübingen, Germany
5. John von Neumann Institute for Computing (NIC), Jülich Supercomputing Centre (JSC), Institute of Biological Information Processing (IBI-7: Structural Biochemistry) & Institute of Bio- and Geosciences (IBG-4: Bioinformatics), Forschungszentrum Jülich GmbH, Jülich, Germany
6. Institute for Pharmaceutical and Medicinal Chemistry, PharmaCampus, Westphalian Wilhelms University, Münster, Germany
7. Department of Pediatrics, Pediatric Hematology and Oncology, University Hospital Carl Gustav Carus, Dresden, Germany
8. National Center for Tumor Diseases (NCT), Partner Site Dresden, Dresden, Germany
9. Pharmaceutical and Cell Biological Chemistry, Pharmaceutical Institute University of Bonn, Bonn, Germany
10. Institute of Biochemistry, Heinrich Heine University Düsseldorf, Düsseldorf, Germany

* contributed equally to this work

\# shared senior authorship

\# **Corresponding authors:** (T.K.) Universitätsstr. 1, 40225 Düsseldorf, Germany, Phone: (+49) 211 81 14984, E-mail: thomas.kurz@uni-duesseldorf.de; (H.G.) Universitätsstr. 1, 40225 Düsseldorf, Germany, Phone: (+49) 211 81 13662, E-mail: gohlke@uni-dueseldorf.de; (S.B.) Moorenstraße 5, 40225 Düsseldorf, Germany, Phone (+49) 211 81 04896 Email, sanil.bhatia@med.uni-duesseldorf.de

Table of Contents

1. Chemical Synthesis

All solvents and chemicals were used as purchased without further purification. The progress of all reactions was monitored on silica gel plates (with fluorescence indicator UV254) using the solvent system stated. Flash column chromatography was carried out using CombiFlash® 200 (Teledyne Isco) and prepacked RediSep® (NP) silica cartridges. Melting points (Mp) were taken in open capillaries and are uncorrected. ^{1}H and ^{13}C spectra were recorded on Avance™ DRX-500 (Bruker) (^{1}H 500 MHz; ^{13}C 126 MHz) and Avance™ III–600 (Bruker) (^{1}H 600 MHz; ^{13}C 151 MHz) spectrometers, respectively, using DMSO-d_6 or Chlorodorm-*d* as solvents. Chemical shifts are given in parts million (ppm), (δ relative to residual solvent peak for ^{1}H and ^{13}C or to external standard tetramethylsilane). Elemental analysis (CHN) was performed with a Perkin Elmer PE 2400 CHN Elemental Analyzer. Azlactone **I** was prepared as reported by MATOS *et al*. and crystallized from isopropyl alcohol.[1] Amidine hydrochlorides **IIa** and **IIb** were prepared following a literature procedure by MARTINU *et al*. with the minor modification using 0.6 equiv. of the corresponding amine hydrochloride.[2] The preparation of the pyrimidone monomers **1**, **2a**, **2b**, **2e**, dimers **3**, **4** and tripyrimidonamide **5a** was previously reported by us.[3]

*Synthesis of pyrimidone monomers **III - IV***

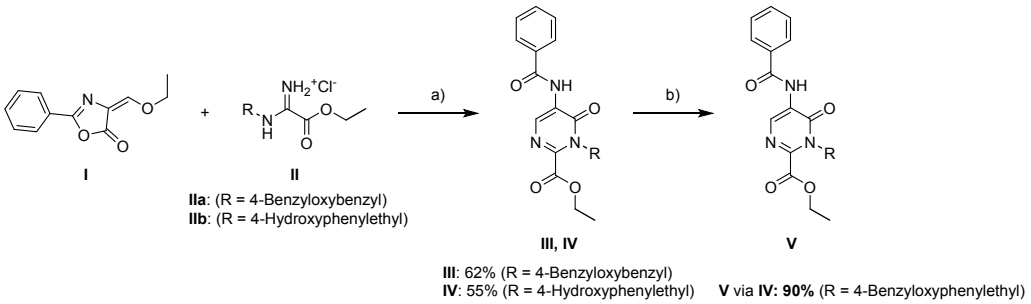

Scheme 1. Synthesis of the pyrimidones **III-V:** a) NEt_3, acetonitrile, reflux, 6 h; b) K_2CO_3, KI, benzyl bromide, acetonitrile, 60°C, 3h.

*General procedure for the synthesis of pyrimidone monomers **III** and **IV**.*

A mixture of 4-ethoxymethylene-2-phenyl-2-oxazolin-5-one **I** (0.217 g, 1 mmol), the respective amidine hydrochloride **IIa** or **IIb** (1 mmol) and triethylamine (0.101 g, 1 mmol) in dry acetonitrile (5 mL) was heated under a nitrogen atmosphere for 6 h. The solvent was removed under reduced pressure, and aqueous citric acid (10 wt %, 3 mL) was added. The mixture was extracted with ethyl acetate (3 × 30 mL), the combined organic layers were dried over anhydrous sodium sulfate, filtered and concentrated under vacuum. The crude products were purified by flash column chromatography (gradient: 10:90 → 30:70 ethyl acetate : *n*-hexane) to yield monomeres **III** and **IV**.

Pyrimidone monomer III

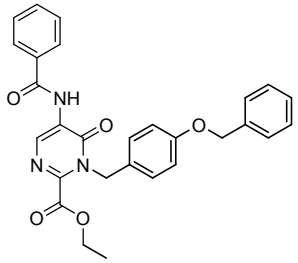

$C_{28}H_{25}N_3O_5$
483,52 g/mol

Yield: 62% (299 mg, 0.62 mmol), yellow crystalline solid.

Mp: 109 °C (dichloromethane).

^{1}H NMR (600 MHz, DMSO-d_6) δ 9.58 (s, 1H), 8.81 (d, J = 3.9, 1H), 8.18 – 7.85 (m, 2H), 7.71 – 7.60 (m, 1H), 7.55 (t, J = 7.7, 2H), 7.43 (d, J = 7.4, 2H), 7.38 (t, J = 7.5, 2H), 7.32 (t, J = 7.3, 1H), 7.17 (d, J = 8.7, 2H), 7.01 – 6.95 (m, 2H), 5.30 (s, 2H), 5.03 (d, J = 73.9, 2H), 4.28 (q, J = 7.1, 2H), 1.36 – 1.07 (t, 3H).

^{13}C NMR (151 MHz, DMSO-d_6) δ 165.48, 160.44, 157.83, 156.77, 144.72, 136.95, 133.14, 132.35, 128.84, 128.67, 128.39, 127.79, 127.69, 127.63, 127.58, 127.56, 114.83, 69.14, 62.91, 47.52, 13.53.

CHN: Calculated [%]: C, 69.55; H, 5.21; N, 8.69 Found [%]: C, 69.60; H, 5.41; N, 8.53.

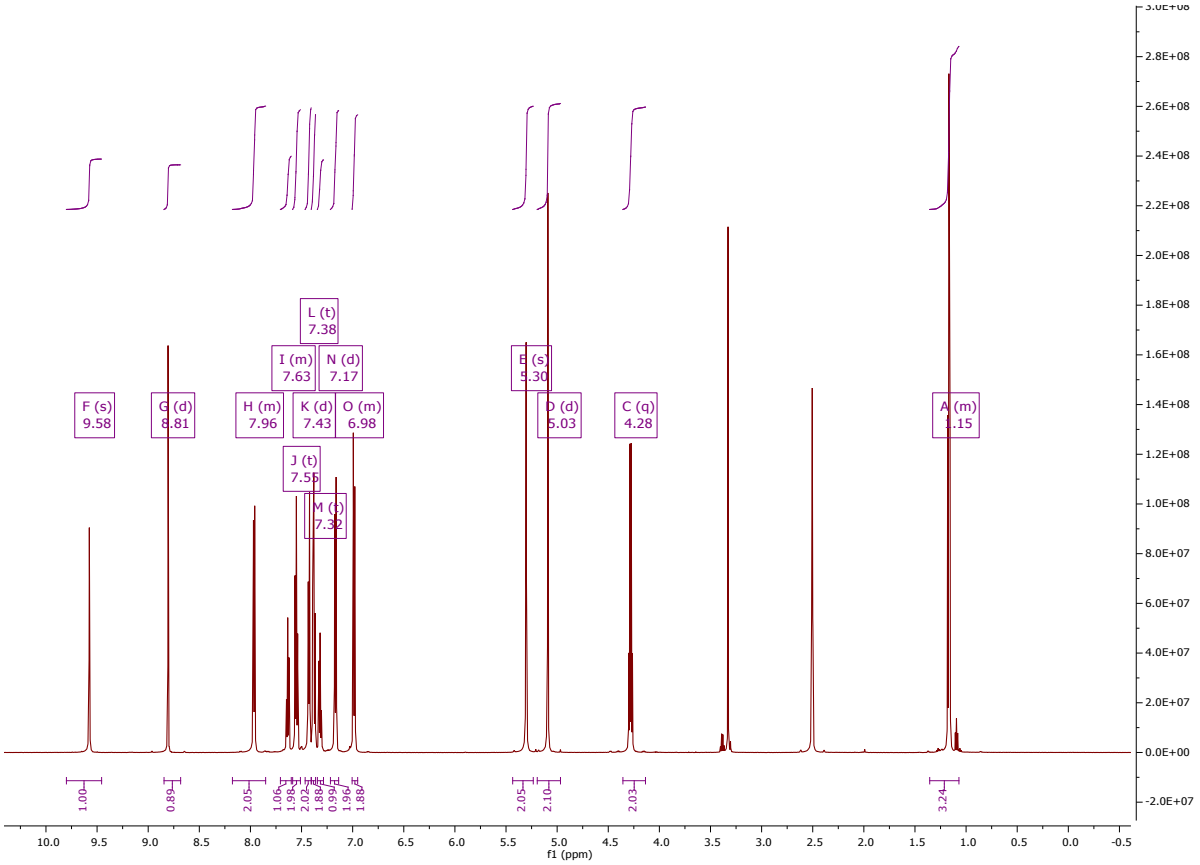

Figure S1. ^{1}H-NMR (600 MHz, DMSO- d_6) of **III** at room temperature.

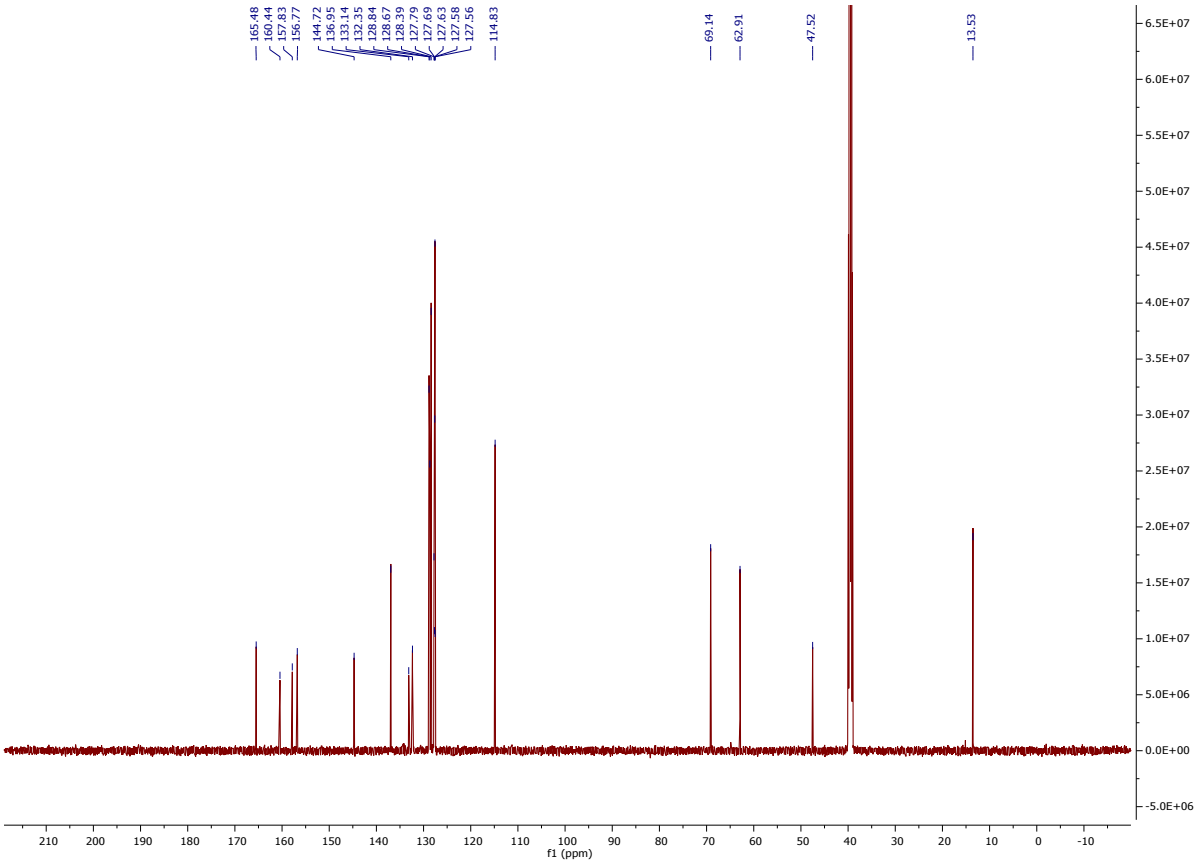

Figure S2. ^{13}C-NMR (151 MHz, DMSO-d_6) of **III** at room temperature.

Pyrimidone monomer IV

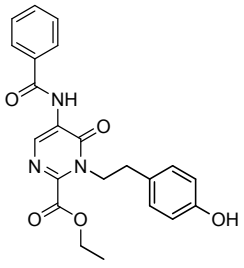

$C_{22}H_{21}N_3O_5$
407,43 g/mol

Yield: 55% (224 mg, 0.55 mmol), yellow crystalline solid.

Mp: 191 °C (dichloromethane).

·**^{1}H NMR** (500 MHz, DMSO-d_6) δ 9.57 (s, 1H), 9.30 (s, 1H), 8.79 (s, 1H), 7.98 (d, J = 8.4, 2H), 7.65 (t, J = 7.3, 1H), 7.57 (t, J = 7.6, 2H), 6.95 (d, J = 8.3, 2H), 6.70 (d, J = 8.4, 2H), 4.35 – 4.23 (m, 5H), 3.33 (s, 1H), 2.92 – 2.84 (m, 2H), 2.54 – 2.49 (m, 2H), 1.30 (t, J = 7.1, 3H).

^{13}C NMR (126 MHz, DMSO-d_6) δ 165.39, 160.34, 156.61, 156.12, 144.14, 136.51, 133.10, 132.32, 129.56, 128.65, 127.56, 127.43, 127.28, 115.39, 62.88, 47.49, 32.92, 13.56.

CHN: Calculated [%]: C, 64.86; H, 5.20 N, 10.31 Found [%]: C 64.71; H, 5.22; N, 10.25.

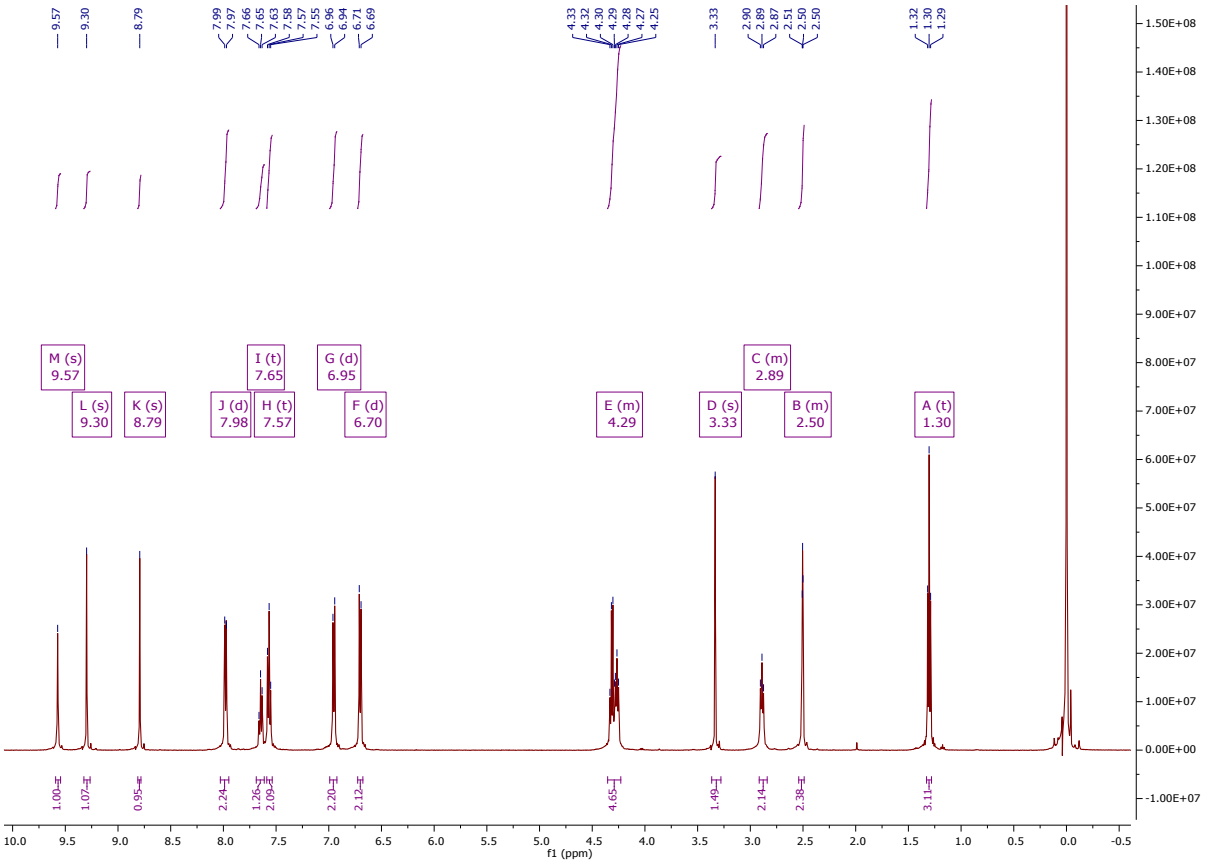

Figure S3. ^{1}H-NMR (500 MHz, DMSO-d_6) of **IV** at room temperature.

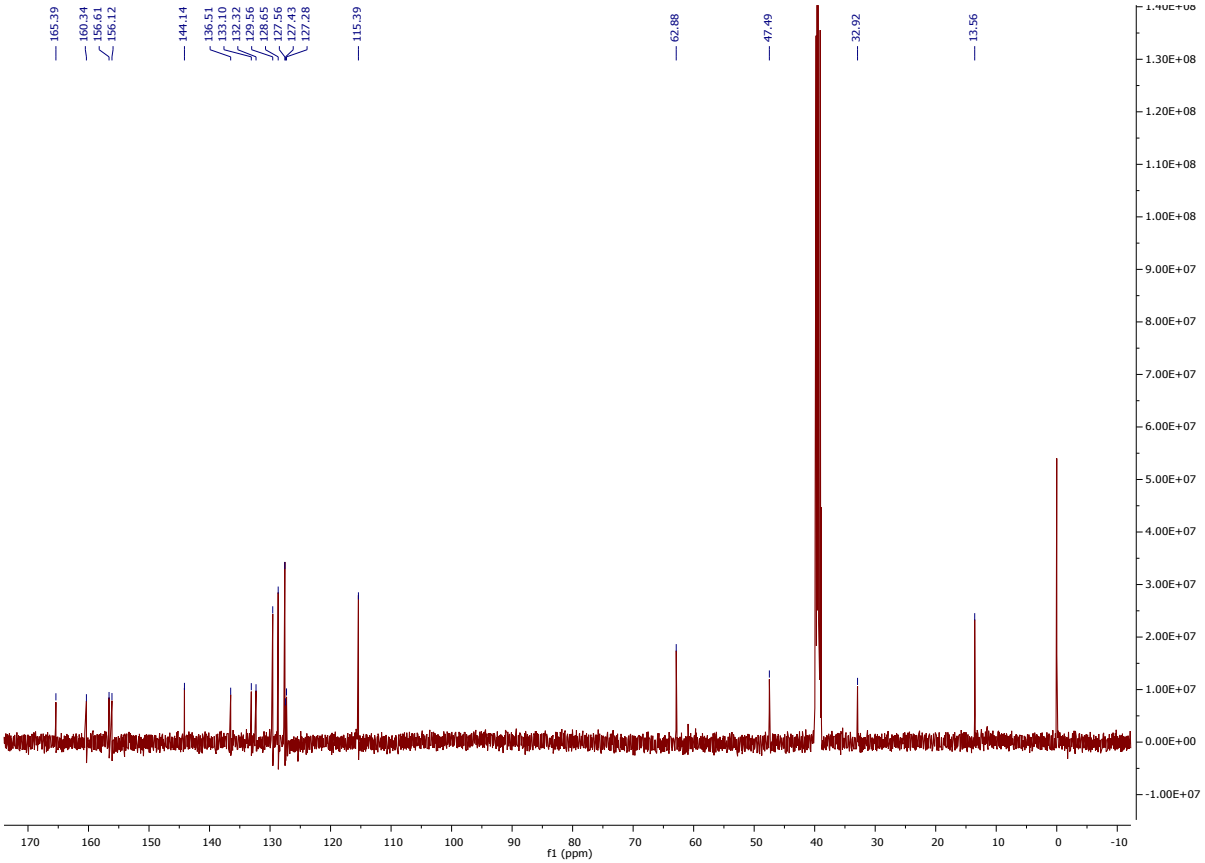

Figure S4. ^{13}C-NMR (126 MHz, DMSO-d_6) of **IV** at room temperature.

*Procedure for the synthesis of pyrimidone monomer **V***

To a suspension of **IV** (0.407 g, 1.0 mmol), potassium carbonate (0.207 g, 1.5 mmol) and potassium iodide (0.166 g) in acetonitrile (2 mL) benzyl bromide (0.342 g, 2.0 mmol) was added dropwise under stirring. The suspension was stirred at 60 °C for 3 h under an argon atmosphere. Subsequently dichloromethane (10 mL) and water (10 mL) was added and the stirring was continued until a phase separation was observed. The organic phase was separated and dried over sodium sulfate. After filtration the solvent was removed under reduced pressure and the resulting oil was treated with diethyl ether to initiate crystallization. The solid was separated by filtration and purified by recrystallization from dichloromethane.

Pyrimidone monomer V

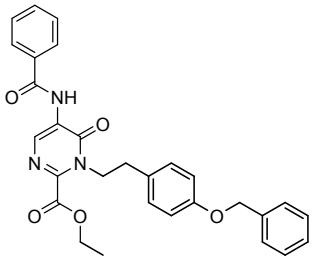

Yield: 90% (403 mg, 0.81 mmol), yellow crystalline solid.

Mp: 83 °C (dichloromethane).

^{1}H NMR (600 MHz, chloroform-*d*) δ 9.20 (s, 1H), 8.98 (s, 1H), 7.94 (m, 2H), 7.59 (d, *J* = 7.4, 1H), 7.52 (t, *J* = 7.7, 2H), 7.40 (m, 4H), 7.33 (d, *J* = 7.2, 1H), 7.13 (d, *J* = 8.6, 2H), 6.93 (m, 2H), 5.05 (s, 2H), 4.47 (m, 2H), 4.38 (q, *J* = 7.2, 2H), 3.04 (m, 2H), 1.41 (t, *J* = 7.2, 3H).

^{13}C NMR (151 MHz, chloroform-*d*) δ 165.63, 160.63, 157.90, 157.40, 142.76, 136.94, 134.73, 133.34, 132.63, 130.05, 129.49, 128.96, 128.61, 128.05, 128.01, 127.48, 127.36, 115.19, 70.02, 63.42, 47.89, 33.99, 13.96.

CHN: Calculated [%]: C, 70.01; H, 5.47; N, 8.45 Found [%]: C, 69.89; H, 5.44; N, 8.56.

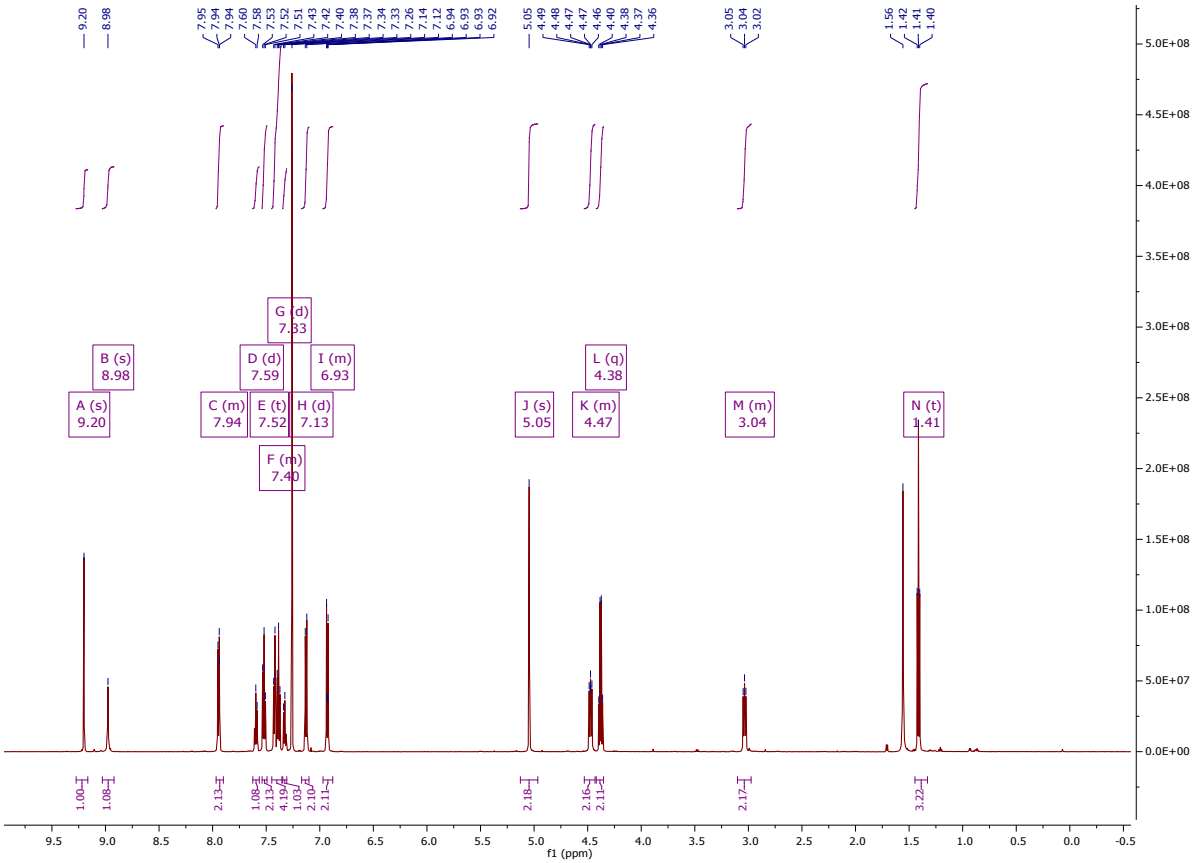

Figure S5. ^{1}H-NMR (500 MHz, Chloroform-d) of **V** at room temperature.

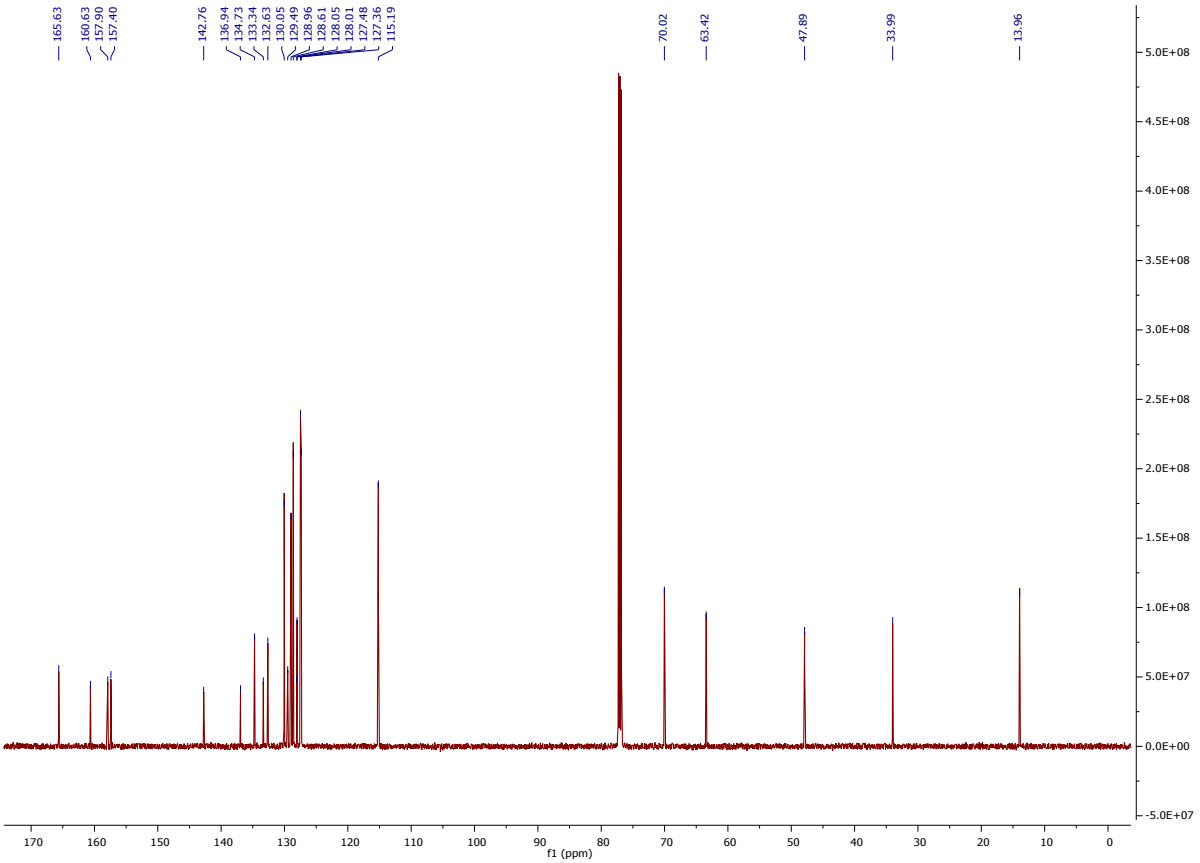

Figure S6. ^{13}C-NMR (151 MHz, Chloroform-d) of **V** at room temperature.

*Synthesis of dimeric pyrimidonamides (**3** ,**4**)[3] and tripyrimidonamides (**5a**[3]**-5d**)*

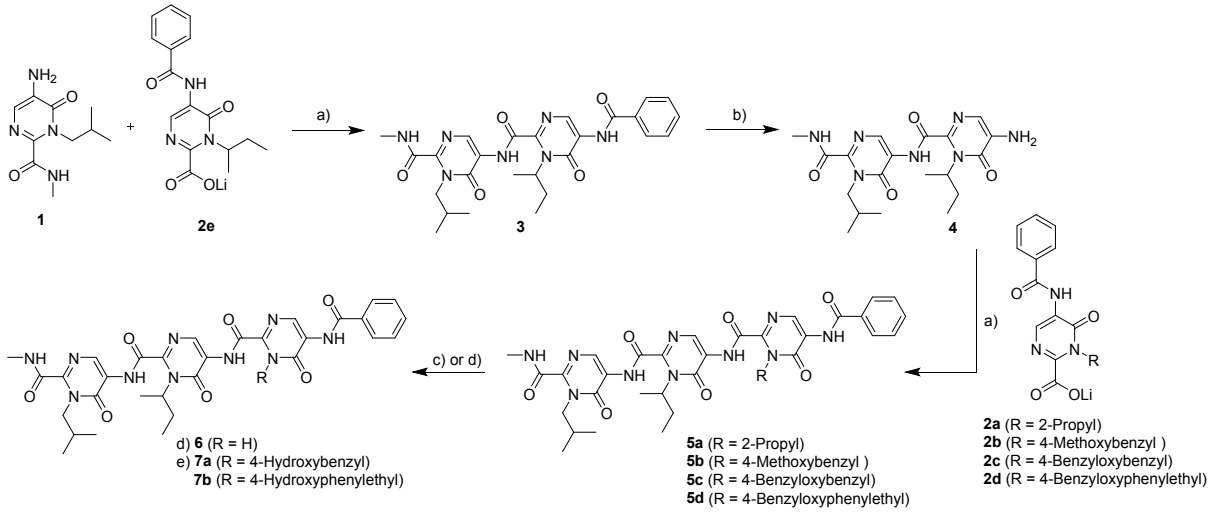

Scheme 2. Synthesis of tripyrimidon amides: a) COMU, DMF, r. t., 18 h; b) NaOH, MeOH, 80 °C, 6 h; c) via **5b**, BBr_3, DCM, -78 °C, 1 h, r. t., 1 h; d) via **5c** and **5d**, H_2, Pd(C), MeOH, DCM, r. t., 1 h.

*General procedure for synthesis the dimeric 5 aminopyrimidonamide (**4**)* [3]

A mixture of the dipyrimidonamide **3** (1 mmol, obtained from monomer **1** and lithium carboxylate **2e** according to[3]) and sodium hydroxide (0.12 g, 3 mmol) in methanol 3 mL) was heated for 6 h. The solvent was removed under reduced pressure, water (5 mL) was added, and the aqueous layer was extracted with ethyl acetate (3 × 15 mL). The combined organic layers were dried over sodium sulfate, filtered and concentrated under reduced pressure. The crude residue was purified by flash column chromatography (gradient: 30:70 → 100:0 ethyl acetate:*n*-hexane) to yield **4** (77%).

*General procedure for synthesis of tripyrimidonamides (**5a-5d**)*

The preparation tripyrimidonamide **5a** was previously reported.[3]

The appropriate ethyl 5-benzamido-6-oxo1,6-dihydropyrimidine-2-carboxylate (**III, V**, 1.5 equiv.) and lithium hydroxide hydrate (1.5 equiv) were dissolved in methanol and stirred for 12 h at room temperature. The solvent was removed under vacuum using an ice cooled water bath. The resulting yellow oil was treated with dry diethyl ether to initiate crystallisation. The precipitate was filtrated off, dried under vacuum to obtain the novel lithium carboxylates **2c, 2d**.

Next, the respective lithium carboxylate (1 mmol, **2a**-**2d**) was transferred into a two-neck round-bottom flask containing the dimeric 5 aminopyrimidonamide **4** (1 mmol.) and COMU (1.8 equiv.). The mixture was dissolved in dry DMF (1 mL per mmol) and stirred for 18 h under nitrogen atmosphere at ambient temperature. Dichloromethane (40 mL) was added, and the organic layer was washed with saturated sodium bicarbonate solution (10 mL), 10% aqueous citric acid solution (10 mL) and brine (10 mL). After drying over sodium sulfate the organic layer was concentrated in vacuum. The residue was crystallized by treatment with dry diethyl ether and the respective tripyrimidoneamide (**5a-5d)** recrystallized from dichloromethane or *n*-hexane/ethyl acetate 1:1, respectively.

Tripyrimidonamide 5a

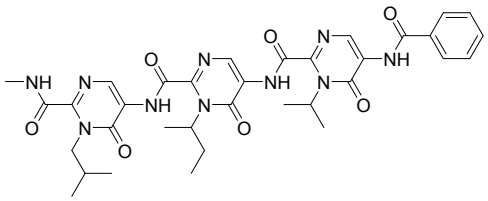

$C_{34}H_{40}N_{10}O_7$
700,76 g/mol

Yield: 65% (455 mg, 0.65 mmol), yellow crystalline solid.

Mp: 257 °C (dichloromethane).

^{1}H NMR (600 MHz, chloroform-*d*) δ 10.17 (s, 1H), 10.05 (s, 1H), 9.09 (s, 1H), 9.03 (s, 1H), 8.95 (s, 1H), 8.93 (s, 1H), 7.96 – 7.91 (m, 2H), 7.69 (q, *J* = 4.5 Hz, 1H), 7.58 (t, *J* = 7.4 Hz, 1H), 7.50 (t, *J* = 7.7 Hz, 2H), 5.49 (hept, *J* = 6.6 Hz, 1H), 5.18 (h, *J* = 6.8 Hz, 1H), 4.67 (d, *J* = 7.3 Hz, 2H), 2.98 (d, *J* = 5.1 Hz, 3H), 2.29 (dp, *J* = 7.5, 15.2 Hz, 1H), 2.10 (hept, *J* = 7.1 Hz, 1H), 1.99 (dp, *J* = 7.3, 14.5 Hz, 1H), 1.70 (d, *J* = 6.8 Hz, 9H), 0.92 (dd, *J* = 1.6, 6.7 Hz, 6H), 0.85 (t, *J* = 7.4 Hz, 3H).

^{13}C NMR (151 MHz, Chloroform-*d*) δ 165.70, 161.04, 158.93, 158.87, 158.46, 158.01, 157.89, 145.14, 144.94, 143.52, 134.44, 133.69, 133.48, 132.98, 132.71, 129.04, 129.02, 128.15, 127.48, 127.05, 60.35, 54.22, 51.15, 28.92, 26.75, 26.00, 19.94, 19.83, 17.98, 11.50.

CHN: Calculated [%]: C, 58.28; H, 5.75; N, 19.99 Found [%]: C, 58.17; H, 5.80; N, 19.85.

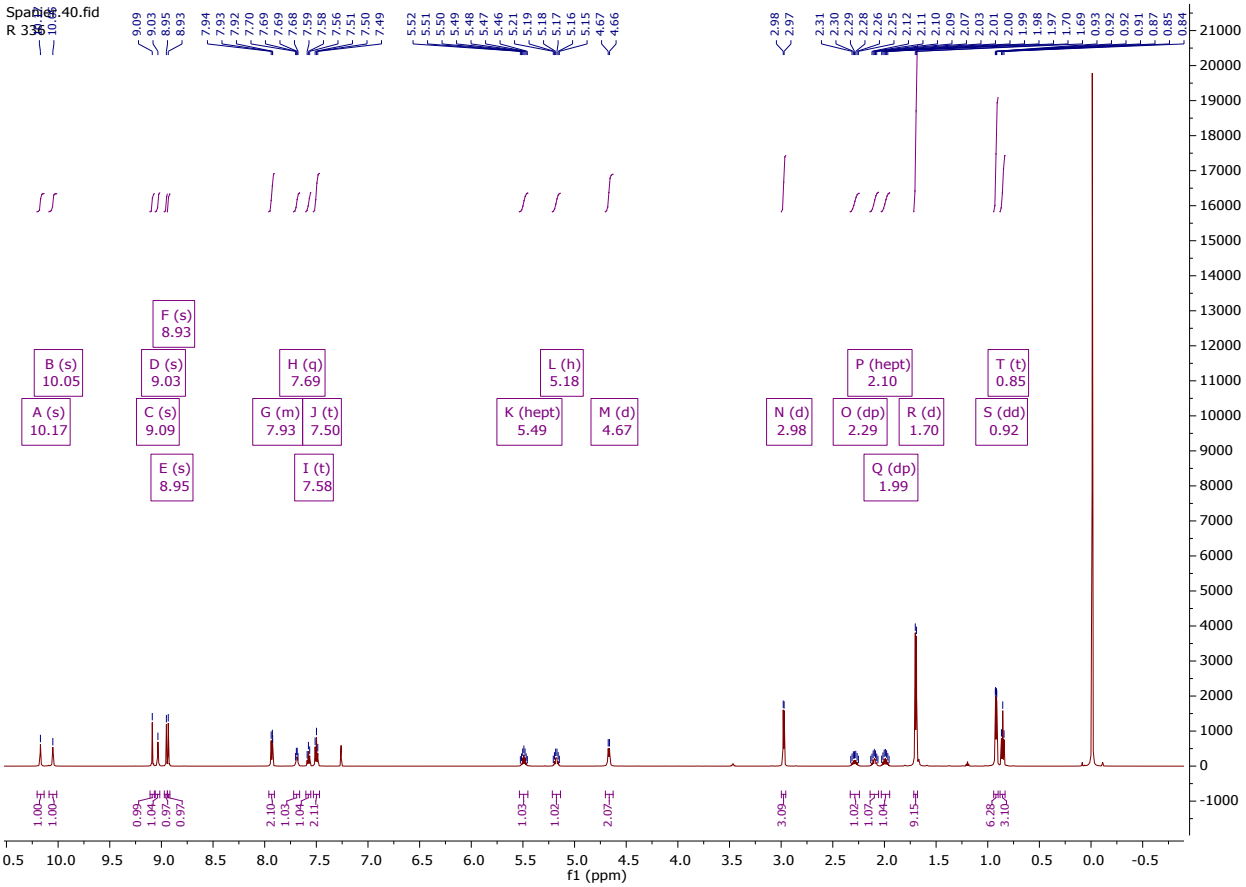

Figure S7. ^{1}H-NMR (600 MHz, , Chloroform-d) of **5a** at room temperature.

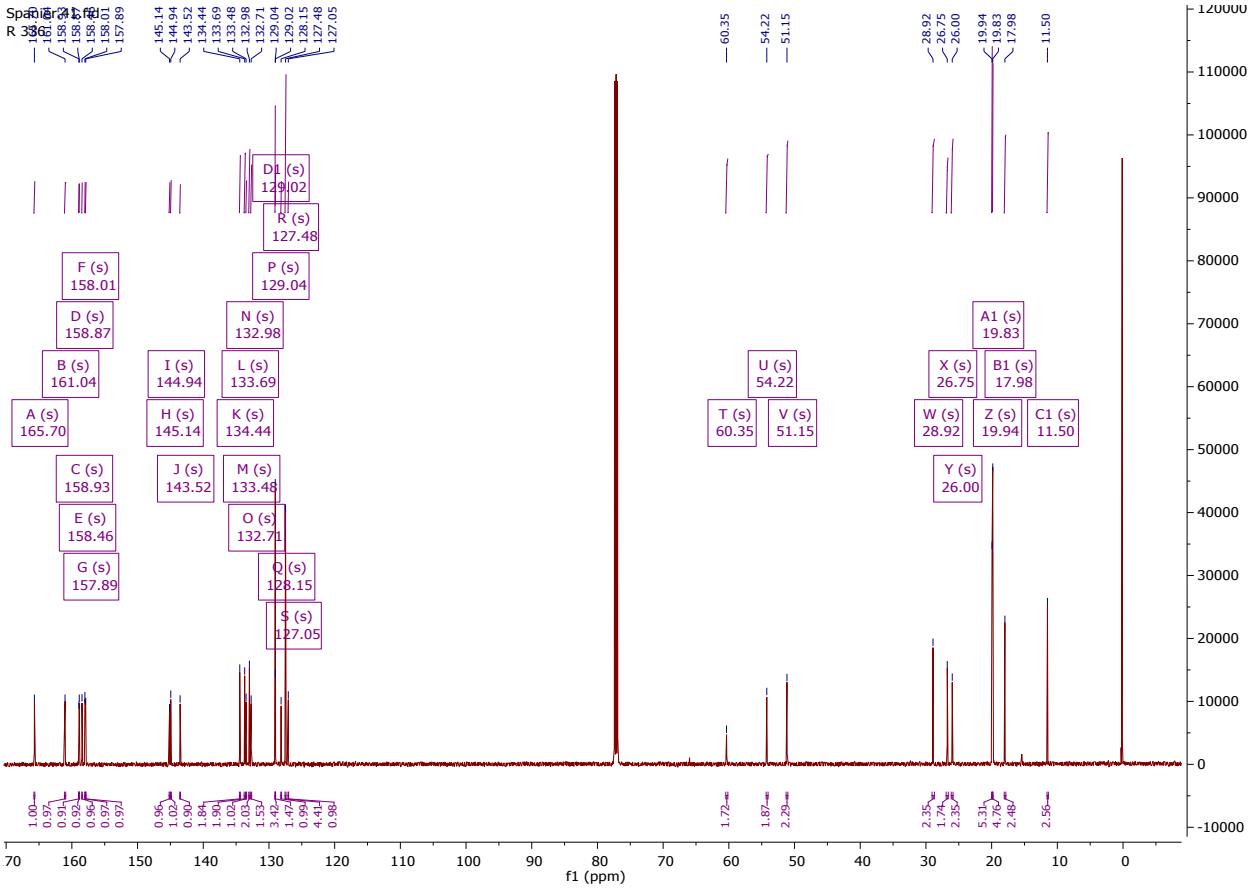

Figure S8. ^{13}C-NMR (151 MHz, Chloroform-d) of **5a** at room temperature.

Tripyrimidonamide 5b

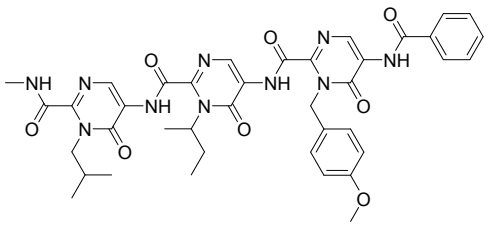

$C_{39}H_{42}N_{10}O_8$
778,83 g/mol

Yield: 39% (152 mg, 0.19 mmol), yellow solid.

Mp: 264 °C (dichloromethane).

^{1}H NMR (600 MHz, chloroform-*d*) δ 10.48 (s, 1H), 10.09 (s, 1H), 9.18 (s, 1H), 9.02 (s, 1H), 8.98 (s, 1H), 8.93 (s, 1H), 7.95 – 7.86 (m, 2H), 7.69 (d, J = 5.0 Hz, 1H), 7.58 (t, J = 7.4 Hz, 1H), 7.50 (t, J = 7.7 Hz, 2H), 7.32 (d, J = 8.8 Hz, 2H), 6.82 (d, J = 8.8 Hz, 2H), 6.00 (s, 2H), 5.28 – 5.09 (m, 1H), 4.67 (d, J = 7.4 Hz, 2H), 3.75 (s, 3H), 2.98 (d, J = 5.1 Hz, 3H), 2.37 – 2.23 (m, 1H), 2.10 (dp, J = 6.9, 13.9 Hz, 1H), 1.98 (td, J = 7.3, 14.4 Hz, 1H), 1.69 (t, J = 9.4 Hz, 3H), 0.92 (dd, J = 1.3, 6.7 Hz, 6H), 0.85 (t, J = 7.4 Hz, 3H).

^{13}C NMR (151 MHz, chloroform-*d*) δ 165.65, 160.93, 159.28, 158.80, 158.27, 158.23, 157.90, 157.74, 144.92, 144.80, 141.33, 134.25, 133.58, 133.41, 133.24, 132.66, 129.73, 128.94, 128.68, 128.22, 127.95, 127.38, 126.93, 114.02, 60.14, 55.23, 51.02, 47.33, 28.81, 26.62, 25.86, 19.82, 17.84, 11.36.

CHN: Calculated [%]: C, 60.15; H, 5.44; N, 17.98 Found [%]: C, 60.15; H, 5.42; N, 17.98.

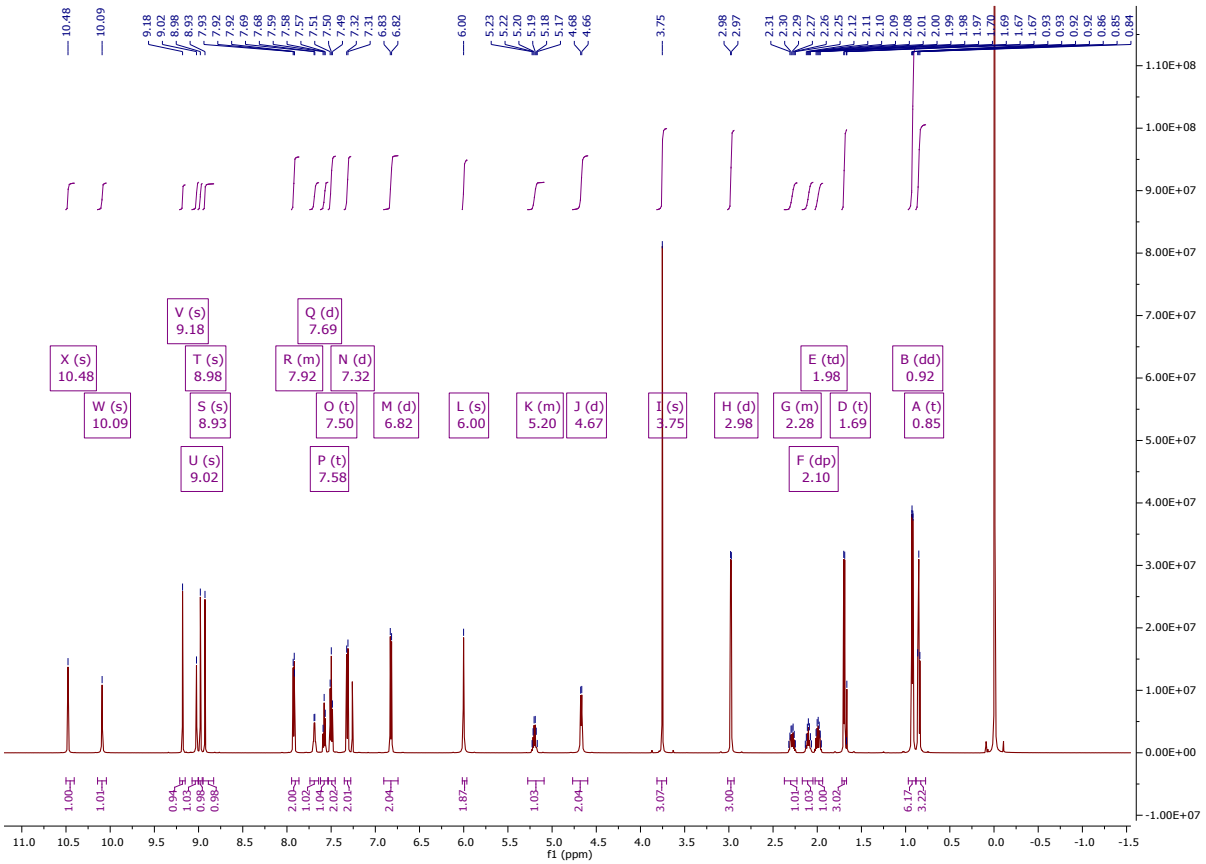

Figure S9. ^{1}H-NMR (600 MHz, , Chloroform-d) of **5b** at room temperature.

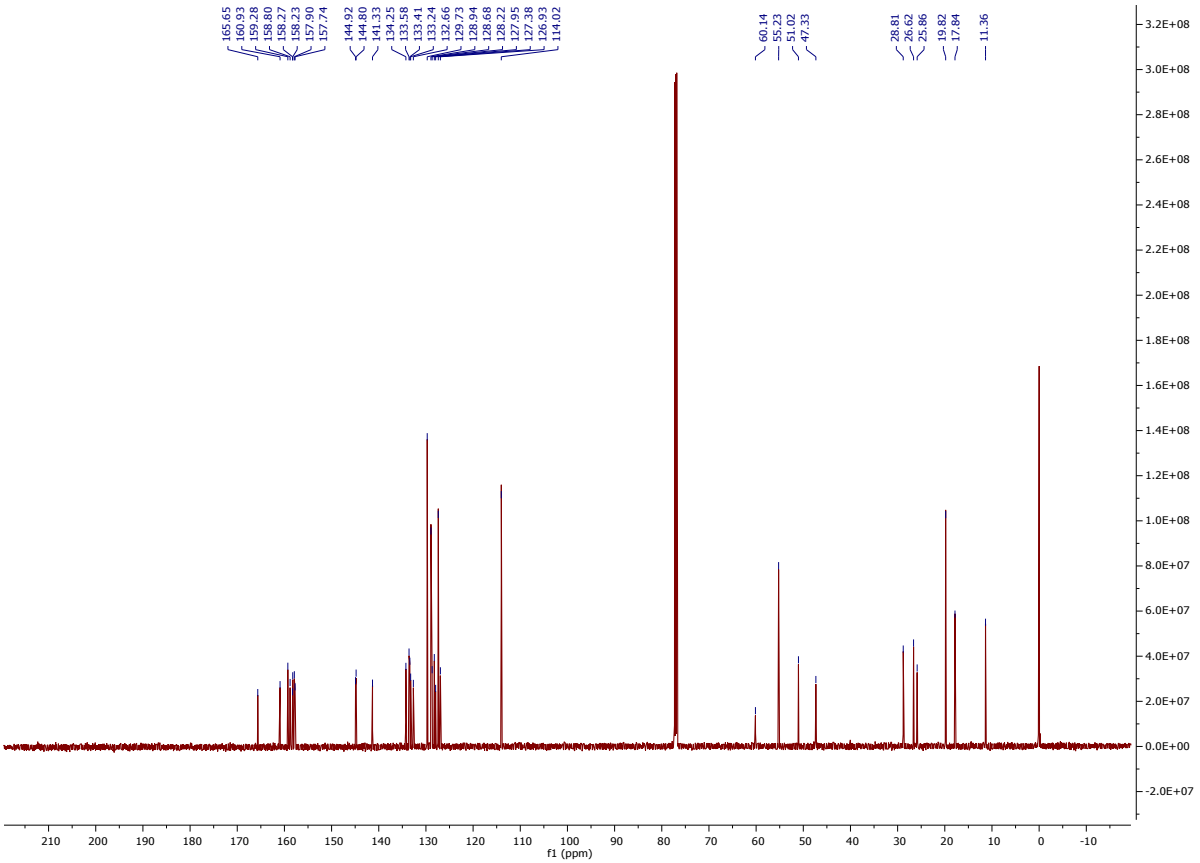

Figure S10. ^{13}C-NMR (151 MHz, Chloroform-d) of **5b** at room temperature.

5c

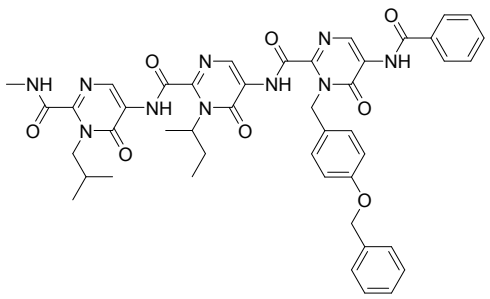

$C_{45}H_{46}N_{10}O_8$
854.93 g/mol

Yield: 71% (455 mg, 0.53 mmol), yellow solid.

Mp: 258 °C (dichloromethane).

^{1}H NMR (600 MHz, chloroform-*d*) δ 10.51 (s, 1H), 10.10 (s, 1H), 9.19 (s, 1H), 9.03 (s, 1H), 8.99 (s, 1H), 8.94 (s, 1H), 7.93 (d, *J* = 7.2 Hz, 2H), 7.67 (q, *J* = 4.2 Hz, 1H), 7.59 (t, *J* = 7.4 Hz, 1H), 7.51 (t, *J* = 7.7 Hz, 2H), 7.42 – 7.27 (m, 7H), 6.91 (d, *J* = 8.7 Hz, 2H), 6.01 (s, 2H), 5.20 (h, *J* = 6.8 Hz, 1H), 5.02 (s, 2H), 4.68 (d, *J* = 7.3 Hz, 2H), 2.98 (d, *J* = 5.1 Hz, 3H), 2.29 (dp, *J* = 7.5, 15.2 Hz, 1H), 2.16 – 2.05 (m, 1H), 2.00 (dp, *J* = 7.4, 14.5 Hz, 1H), 1.70 (d, *J* = 6.7 Hz, 3H), 0.93 (d, *J* = 6.8 Hz, 6H), 0.86 (t, *J* = 7.4 Hz, 3H).

^{13}C NMR (151 MHz, chloroform-*d*) δ 165.81, 161.05, 158.94, 158.64, 158.40, 158.38, 158.05, 157.90, 145.06, 144.91, 141.42, 136.96, 134.39, 133.75, 133.56, 133.38, 132.81, 129.88, 129.08, 128.83,

128.71, 128.62, 128.11, 128.09, 127.58, 127.52, 127.08, 115.08, 70.13, 60.29, 51.17, 47.49, 28.97, 26.77, 26.01, 19.96, 18.00, 11.52.

CHN: Calculated [%]: C, 63.22; H, 5.42; N, 16.38 Found [%]: C, 63.23; H, 5.50; N, 16.14.

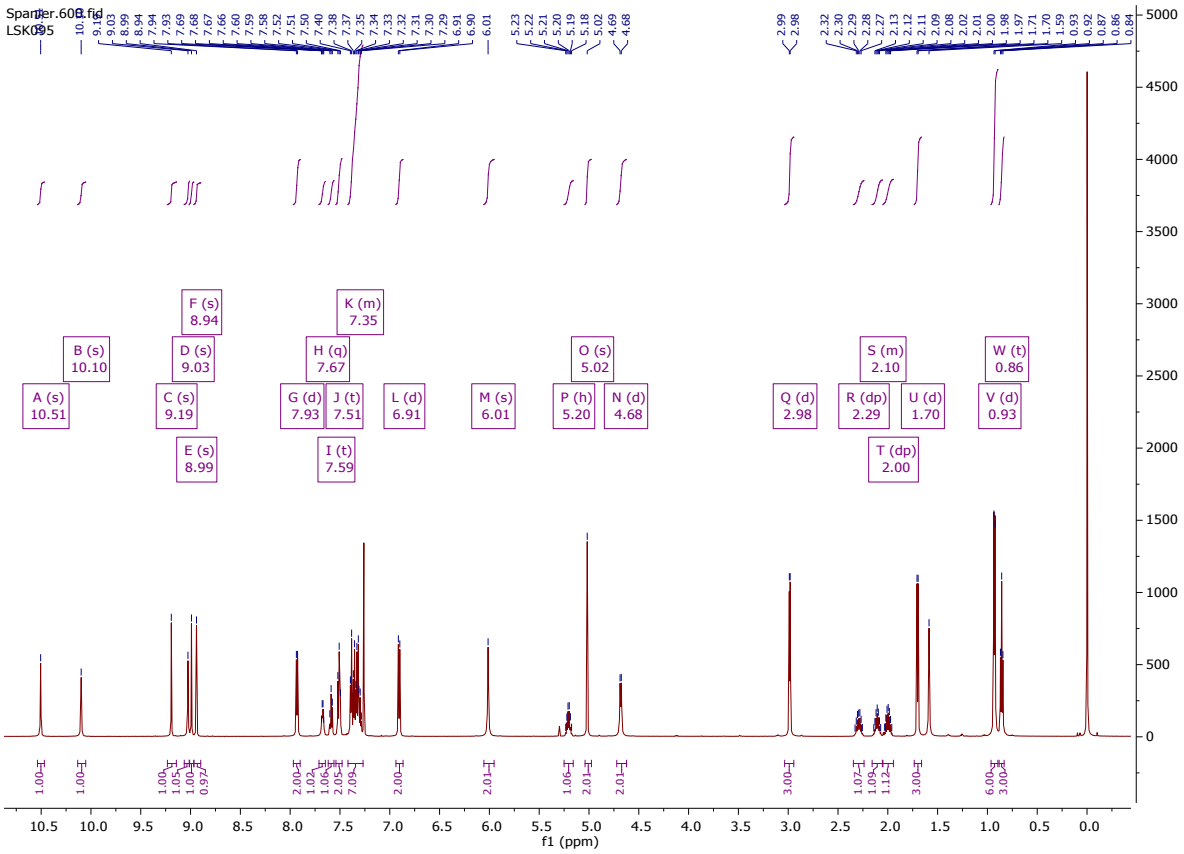

Figure S11. ^{1}H-NMR (600 MHz, , Chloroform-d) of **5c** at room temperature.

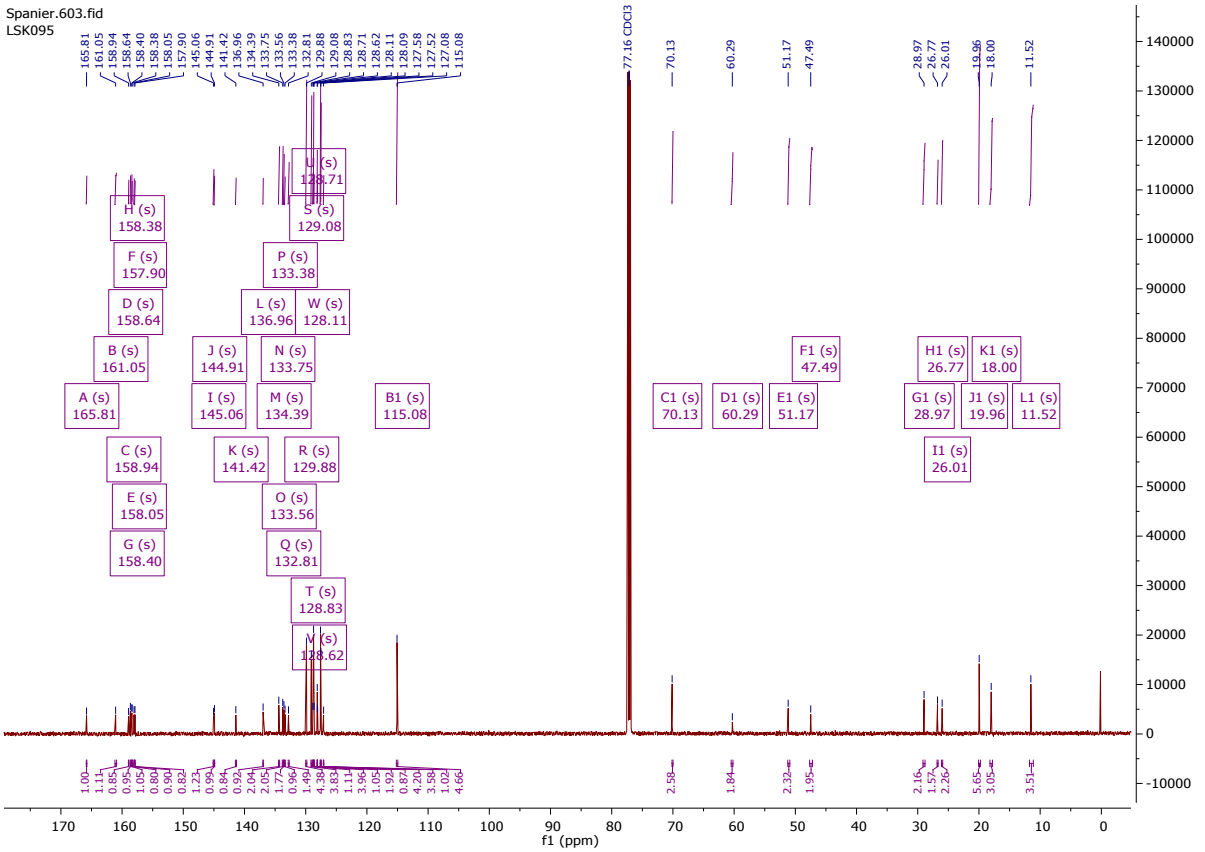

Figure S12. ^{13}C-NMR (151 MHz, Chloroform-d) of **5c** at room temperature.

5d

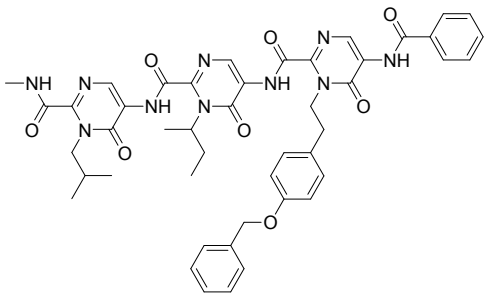

Yield: 76% (330 mg, 0.38 mmol), yellow solid.

Mp: 253 °C (dichloromethane).

^{1}H NMR (600 MHz, chloroform-*d*) δ 10.32 (s, 1H), 10.17 (s, 1H), 9.18 (s, 1H), 9.04 (s, 1H), 9.00 (s, 1H), 8.94 (s, 1H), 7.95 (d, *J* = 7.3 Hz, 2H), 7.68 (q, *J* = 4.7 Hz, 1H), 7.60 (t, *J* = 7.4 Hz, 1H), 7.52 (t, *J* = 7.7 Hz, 2H), 7.41 (d, *J* = 7.2 Hz, 2H), 7.36 (t, *J* = 7.5 Hz, 2H), 7.30 (t, *J* = 7.2 Hz, 1H), 7.22 (d, *J* = 8.5 Hz, 2H), 6.92 (d, *J* = 8.6 Hz, 2H), 5.23 (h, *J* = 6.8 Hz, 1H), 5.03 (s, 2H), 4.93 – 4.87 (m, 2H), 4.69 (d, *J* = 7.4 Hz, 2H), 3.07 – 3.03 (m, 2H), 2.99 (d, *J* = 5.1 Hz, 3H), 2.27 (dp, *J* = 7.5, 15.2 Hz, 1H), 2.12 (dp, *J* = 6.9, 13.9 Hz, 1H), 1.99 (dp, *J* = 7.4, 14.6 Hz, 1H), 1.68 (d, *J* = 6.7 Hz, 3H), 0.96 – 0.92 (m, 6H), 0.84 (t, *J* = 7.4 Hz, 3H).

^{13}C NMR (151 MHz, chloroform-*d*) δ 165.79, 161.05, 158.89, 158.22, 158.08, 158.05, 157.95, 157.83, 144.90, 144.88, 141.85, 137.17, 134.32, 133.63, 133.61, 133.41, 132.81, 130.40, 129.92, 129.10,

128.67, 128.52, 128.08, 128.00, 127.51, 127.49, 127.08, 115.20, 70.10, 60.19, 51.18, 47.33, 34.47, 28.97, 26.77, 26.04, 19.97, 17.97, 11.50.

CHN: Calculated C, 63.58; H, 5.57; N, 16.2 Found [%]: C, 63.6; H, 5.58; N, 15.84.

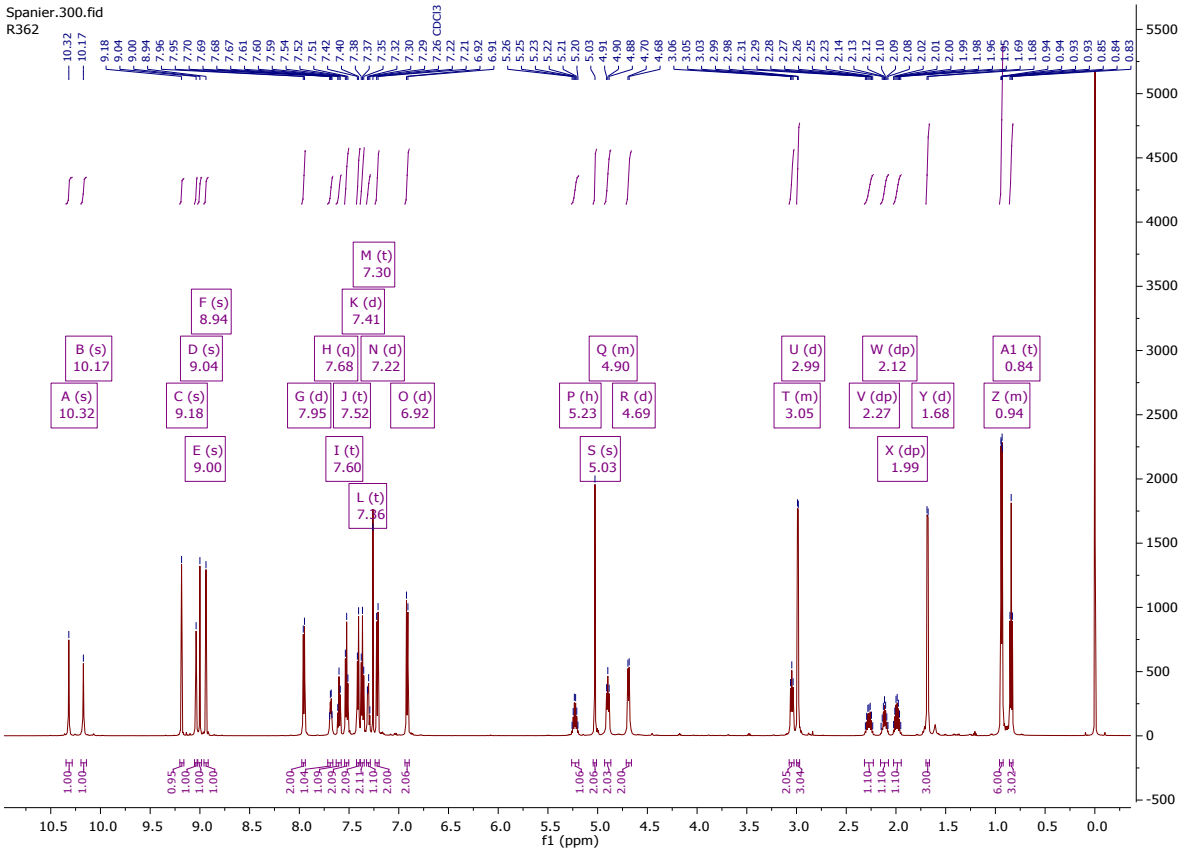

Figure S13. [1]H-NMR (600 MHz, , Chloroform-d) of **5d** at room temperature.

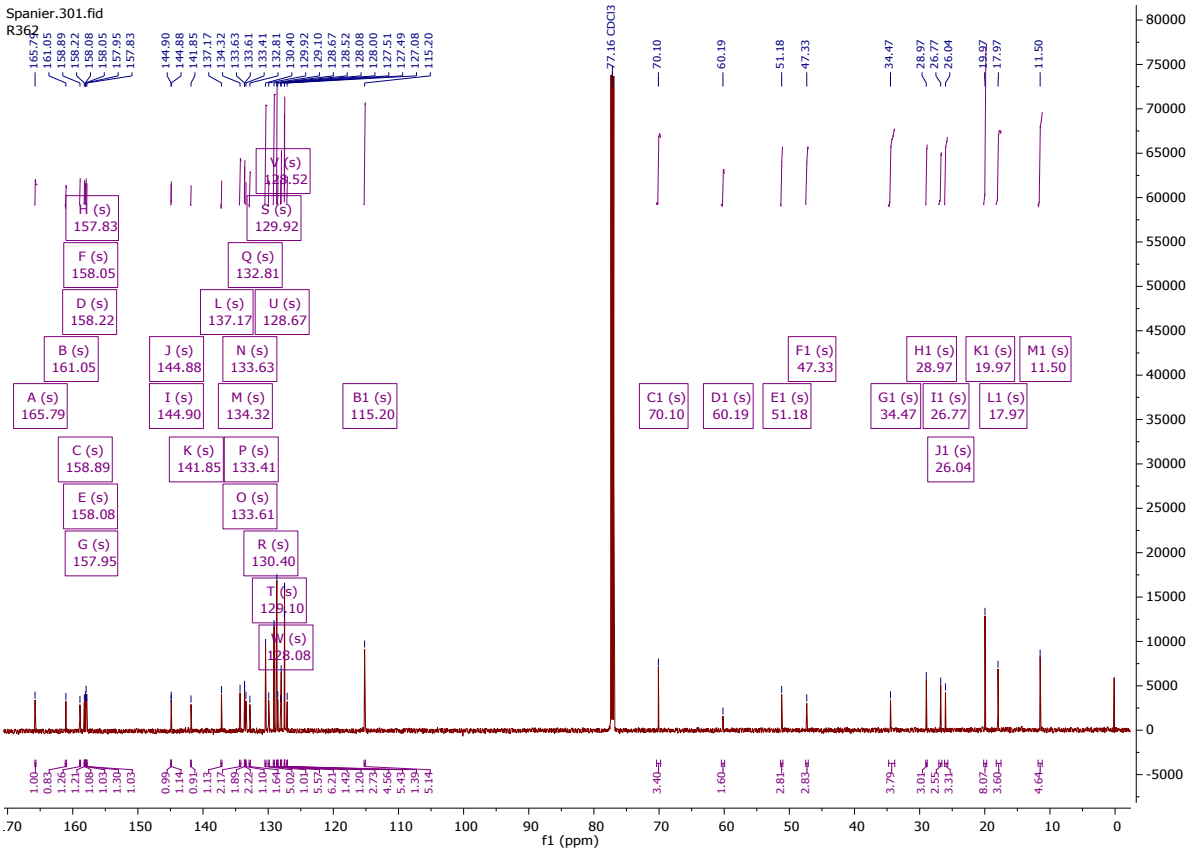

Figure S14. ^{13}C-NMR (151 MHz, Chloroform-d) of **5d** at room temperature.

*Procedure for the synthesis of **6***

A solution of **5b** (85 mg, 0.109 mmol) in dry dichloromethane was cooled to -78 °C using an acetone dry ice bath under an argon atmosphere. Subsequently a 1 M BBr_3 solution in dichloromethane (0.218 mmol, 0.22 ml) was added dropwise to the solution of **5b**. The reaction mixture was stirred at -78 °C for 1 h. After warming to r. t. the stirring was continued for 1 h. The reaction was quenched by adding water (2 ml). After phase seperation the aqueous layer was extracted using dichloromethane (2 x 10 ml) and the combined organic layers were dried over sodium sulfate. After filtration, the solvent was removed under reduced pressure and the resulting solid was recrystallized from dichloromethane to yield the expected tripyrimidonamide.

Tripyrimidonamide 6

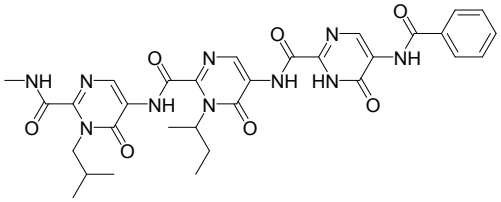

$C_{31}H_{34}N_{10}O_7$
658,68 g/mol

Yield: 65% (30 mg, 0.046 mmol), yellow crystalline solid.

Mp: 253 °C (dichloromethane).

^{1}H NMR (600 MHz, DMSO-d_6/TFA-*d*) δ 10.73 (s, 1H), 10.19 (s, 1H), 9.46 (s, 1H), 8.89 (s, 1H), 8.83 (s, 1H), 8.80 (s, 1H), 7.96 (d, *J* = 7.0 Hz, 2H), 7.63 (t, *J* = 7.4 Hz, 1H), 7.55 (t, *J* = 7.6 Hz, 2H), 4.35 (dd, *J* = 7.4, 11.7 Hz, 1H), 4.15 (d, *J* = 7.4 Hz, 2H), 2.19 (tt, *J* = 7.7, 15.4 Hz, 1H), 2.02 (dt, *J* = 6.7, 13.7 Hz, 1H), 1.91 (tt, *J* = 8.1, 15.0 Hz, 1H), 1.57 (d, *J* = 6.7 Hz, 3H), 0.85 – 0.79 (m, 9H).

^{13}C NMR (151 MHz, DMSO-d_6/TFA-*d*) δ 152.46, 146.24, 138.13, 133.02, 131.03, 58.37, 32.11, 30.02, 29.40, 22.01, 19.75, 13.24.

CHN: Calculated [%]: C, 56.53; H, 5.20; N, 21.27 Found [%]: C, 56.28; H, 5.19; N, 21.06.

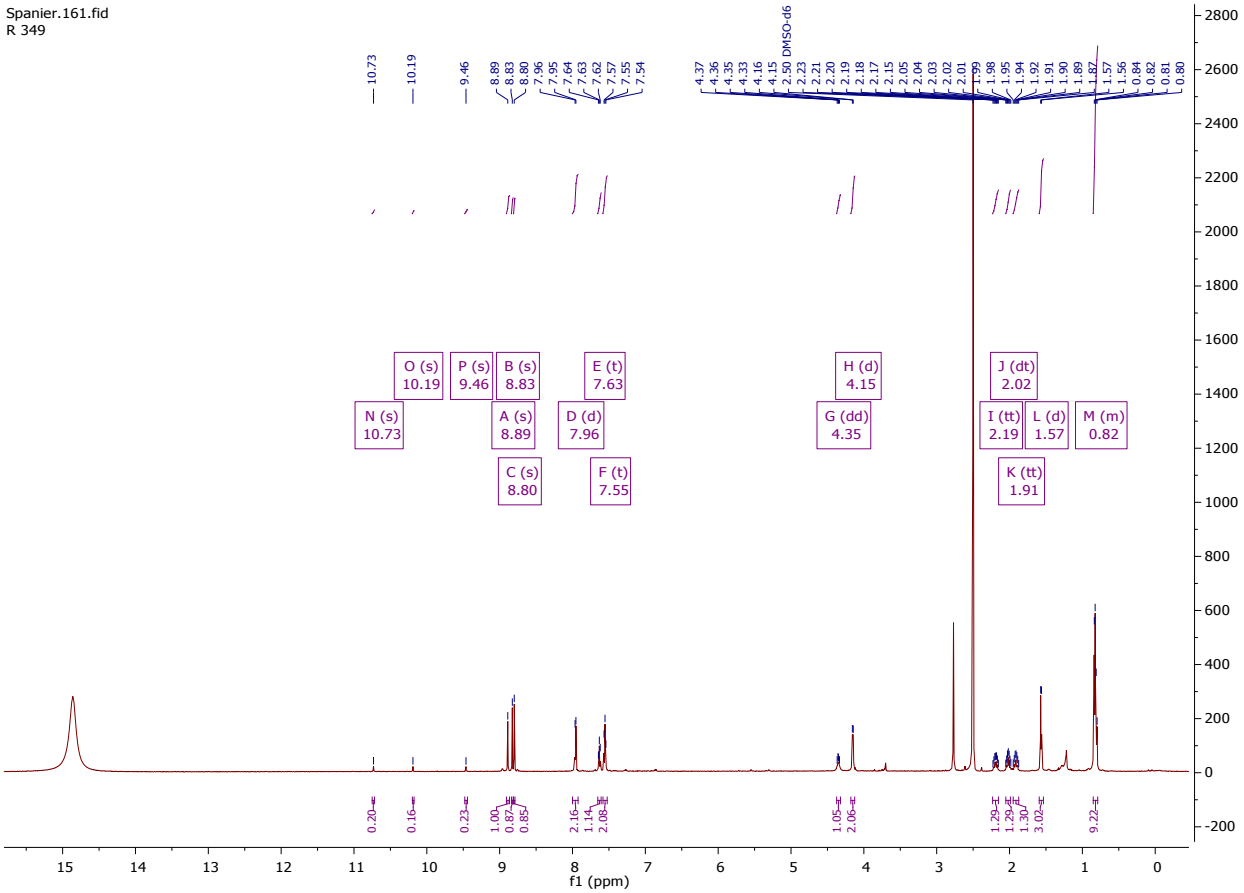

Figure S15. [1]H-NMR (600 MHz, DMSO-d_6/TFA-d) of **6**[1] at room temperature.

[1]Amide protons display weak signals at 9,46 ppm, 10,19 ppm and 10,73 ppm due to a hydrogen deuterium exchange between **6** and TFA-*d*.

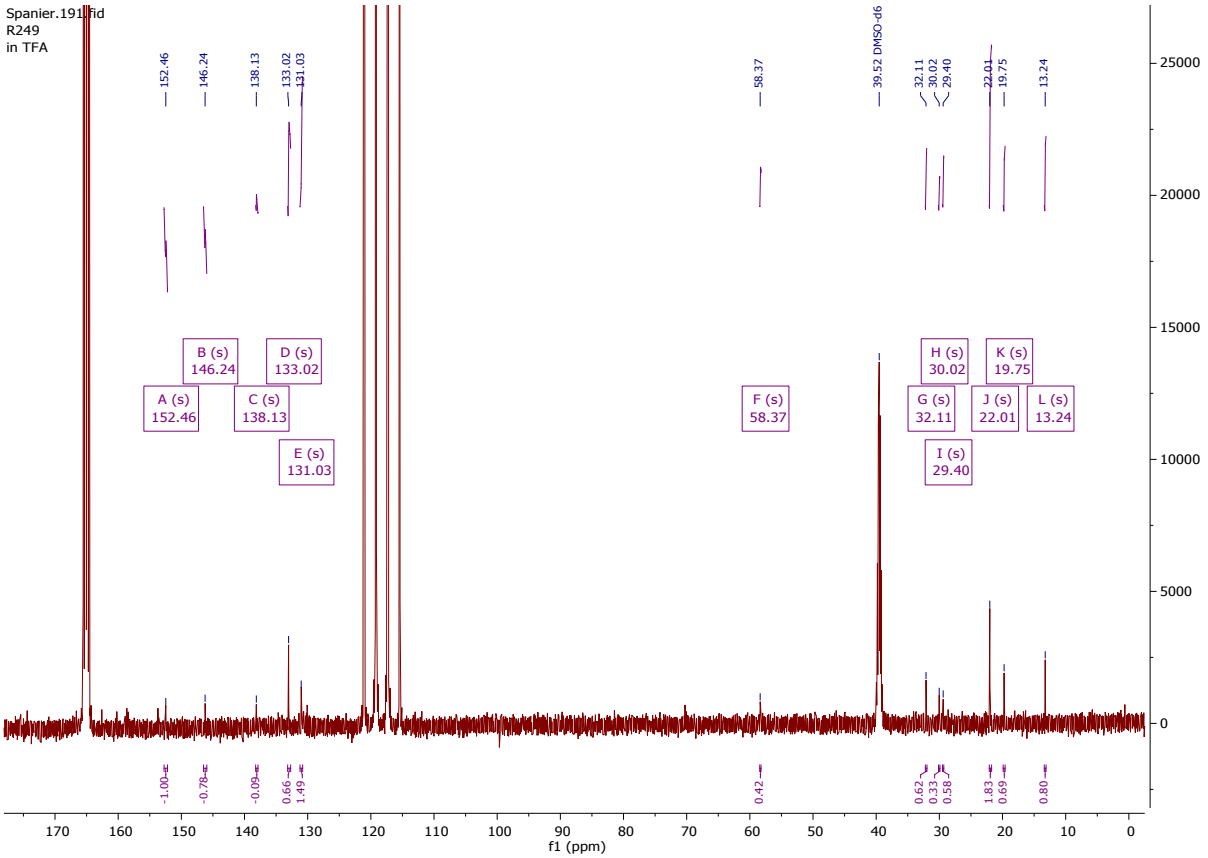

Figure S16. ^{13}C-NMR (151 MHz, DMSO-d_6/TFA-d) of **6**[2] at room temperature.

General procedure for the synthesis of 7a and 7b

The respective benzyl protected tripyrimidonamides **5c** or **5d** (0.25 mmol) and palladium on carbon (10 mg, 10% wt. loading) were suspended in a mixture of dichloromethane and methanol 2:1 (3 ml). The reaction vessel was evacuated and backfilled with hydrogen gas three times. After stirring the reaction mixture at r.t. for 3 h the suspension was filtered through celite and the solvent was removed under reduced pressure. The respective solid (**7a, 7b)** was purified by recrystallization from dichloromethane.

Tripyrimidonamide 7a

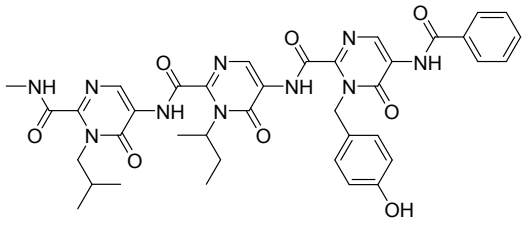

$C_{38}H_{40}N_{10}O_8$
764,80 g/mol

[2] Not all carbon signals were detected.

Yield: 40% (11 mg, 0.015 mmol), yellow solid.

Mp: 226 °C (dichloromethane).

^{1}H NMR (600 MHz, chloroform-*d*) δ 10.49 (s, 1H), 10.10 (s, 1H), 9.20 (s, 1H), 9.03 (s, 1H), 8.99 (s, 1H), 8.93 (d, *J* = 11.8 Hz, 1H), 7.94 (d, *J* = 7.4 Hz, 2H), 7.67 (d, *J* = 4.9 Hz, 1H), 7.59 (t, *J* = 7.4 Hz, 1H), 7.51 (t, *J* = 7.7 Hz, 2H), 7.28 (d, *J* = 8.6 Hz, 2H), 6.76 (d, *J* = 8.6 Hz, 2H), 6.00 (s, 2H), 5.20 (dd, *J* = 7.0, 14.5 Hz, 1H), 4.91 (s, 1H), 4.68 (d, *J* = 7.3 Hz, 2H), 2.98 (t, *J* = 6.1 Hz, 3H), 2.35 – 2.25 (m, 1H), 2.16 – 2.06 (m, 1H), 1.99 (dd, *J* = 7.1, 14.1 Hz, 1H), 1.69 (t, *J* = 9.3 Hz, 3H), 0.92 (t, *J* = 7.2 Hz, 6H), 0.84 (dt, *J* = 7.4, 15.0 Hz, 4H).

^{13}C NMR (151 MHz, chloroform-*d*) δ 165.74, 160.94, 158.81, 158.26, 157.93, 157.76, 155.53, 144.93, 144.80, 141.34, 134.33, 133.63, 133.51, 132.70, 129.94, 129.74, 128.95, 128.67, 128.58, 128.22, 127.94, 127.39, 126.94, 115.51, 60.16, 51.06, 47.35, 28.82, 26.64, 25.87, 19.81, 17.84, 11.37.

CHN: Calculated [%]: C, 56.53; H, 5.20; N, 21.27 Found [%]: C, 56.28; H, 5.19; N, 21.06.

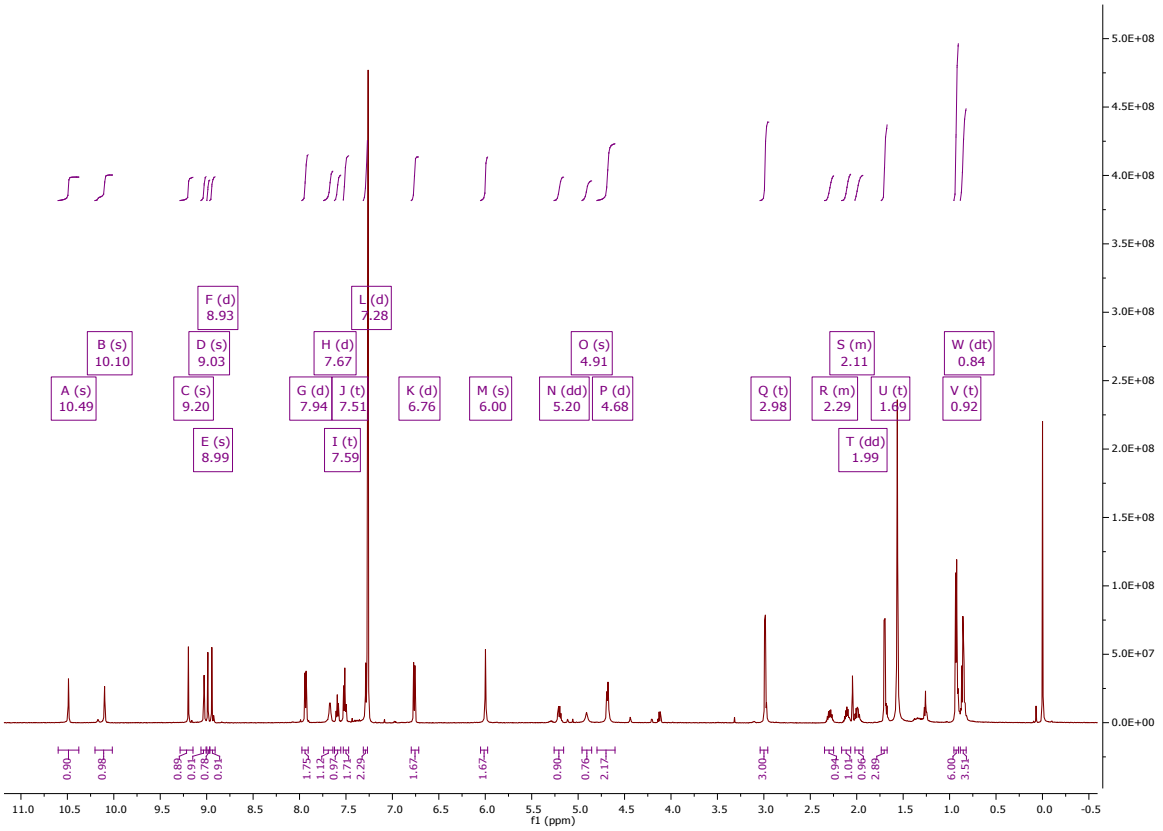

Figure S17. [1]H-NMR (600 MHz, Chloroform-d) of **7a** at room temperature.

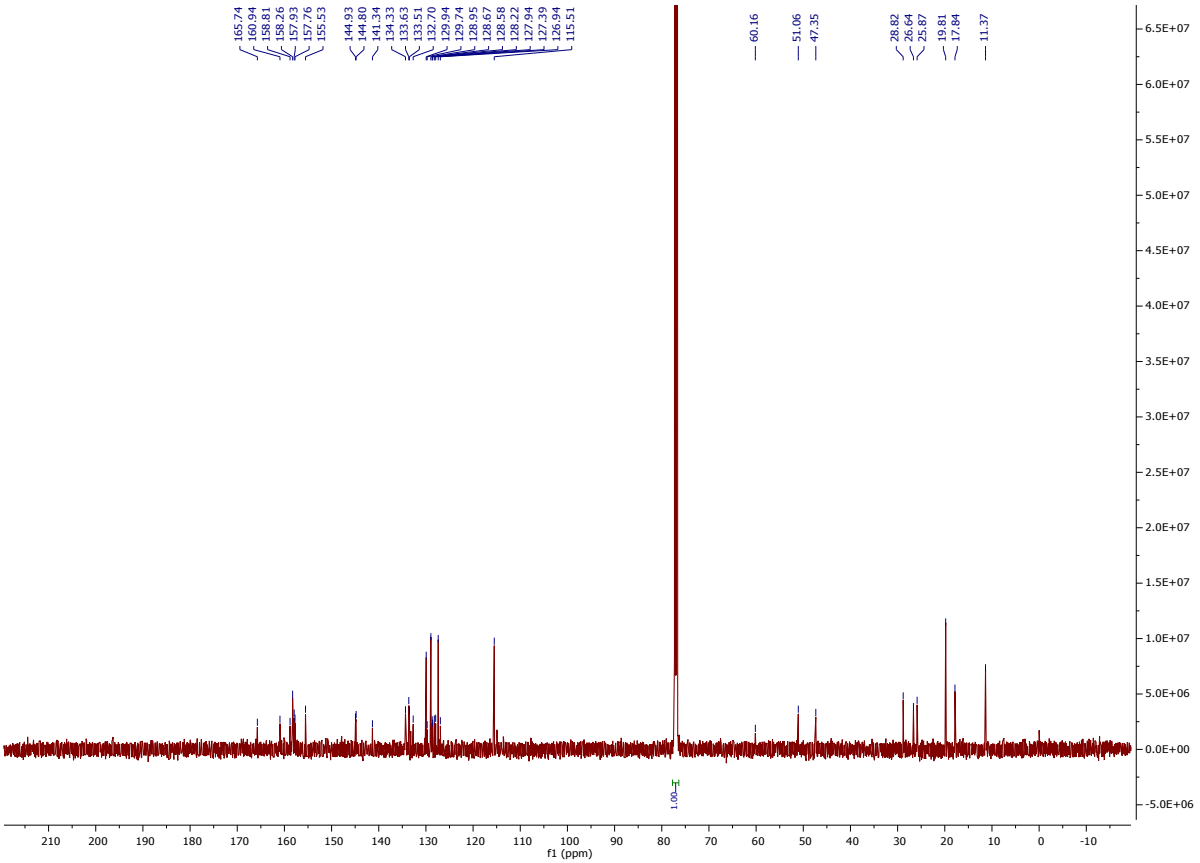

Figure S18. ^{13}C-NMR (151 MHz, Chloroform-d) of **7a** at room temperature.

Tripyrimidoneamide 7b

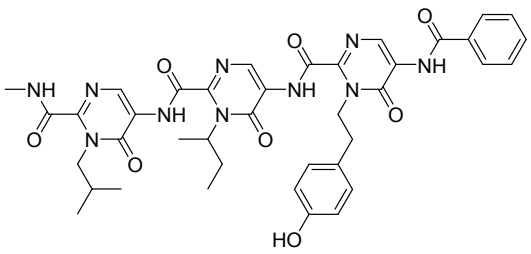

$C_{39}H_{42}N_{10}O_8$
778,83 g/mol

Yield: 87% (81 mg, 0.10 mmol), yellow solid.

Mp: 256 °C (dichloromethane).

^{1}H NMR (600 MHz, DMSO-d_6) δ 10.76 (s, 1H), 10.32 (s, 1H), 9.62 (s, 1H), 9.24 (s, 1H), 8.99 (q, J = 4.6 Hz, 1H), 8.86 (s, 1H), 8.81 (s, 1H), 8.79 (s, 1H), 8.00 (d, J = 7.3 Hz, 2H), 7.66 (t, J = 7.4 Hz, 1H), 7.58 (t, J = 7.6 Hz, 2H), 7.04 (d, J = 8.4 Hz, 2H), 6.69 (d, J = 8.4 Hz, 2H), 4.53 – 4.43 (m, 2H), 4.35 (d, J = 6.2 Hz, 1H), 4.16 (d, J = 7.4 Hz, 2H), 3.04 – 2.84 (m, 2H), 2.79 (d, J = 4.7 Hz, 3H), 2.27 – 2.11 (m, 1H), 2.03 (td, J = 6.9, 13.8 Hz, 1H), 1.92 (dt, J = 7.2, 14.1 Hz, 1H), 1.58 (d, J = 6.7 Hz, 3H), 0.84 (dd, J = 7.2, 16.2 Hz, 9H).

^{13}C NMR (151 MHz, DMSO) δ 165.49, 161.52, 160.41, 158.79, 157.14, 156.78, 156.60, 156.12, 148.69, 148.25, 144.96, 137.13, 136.04, 135.39, 133.16, 132.40, 129.67, 128.72, 127.73, 127.66, 127.36, 126.39, 125.81, 115.35, 50.66, 47.02, 33.41, 27.67, 25.86, 25.36, 19.71, 17.07, 11.01.

HCN: Calculated [%]: C, 60.15; H, 5.44; N, 17.98 Found [%]: C, 59.93; H, 5.46; N, 17.91.

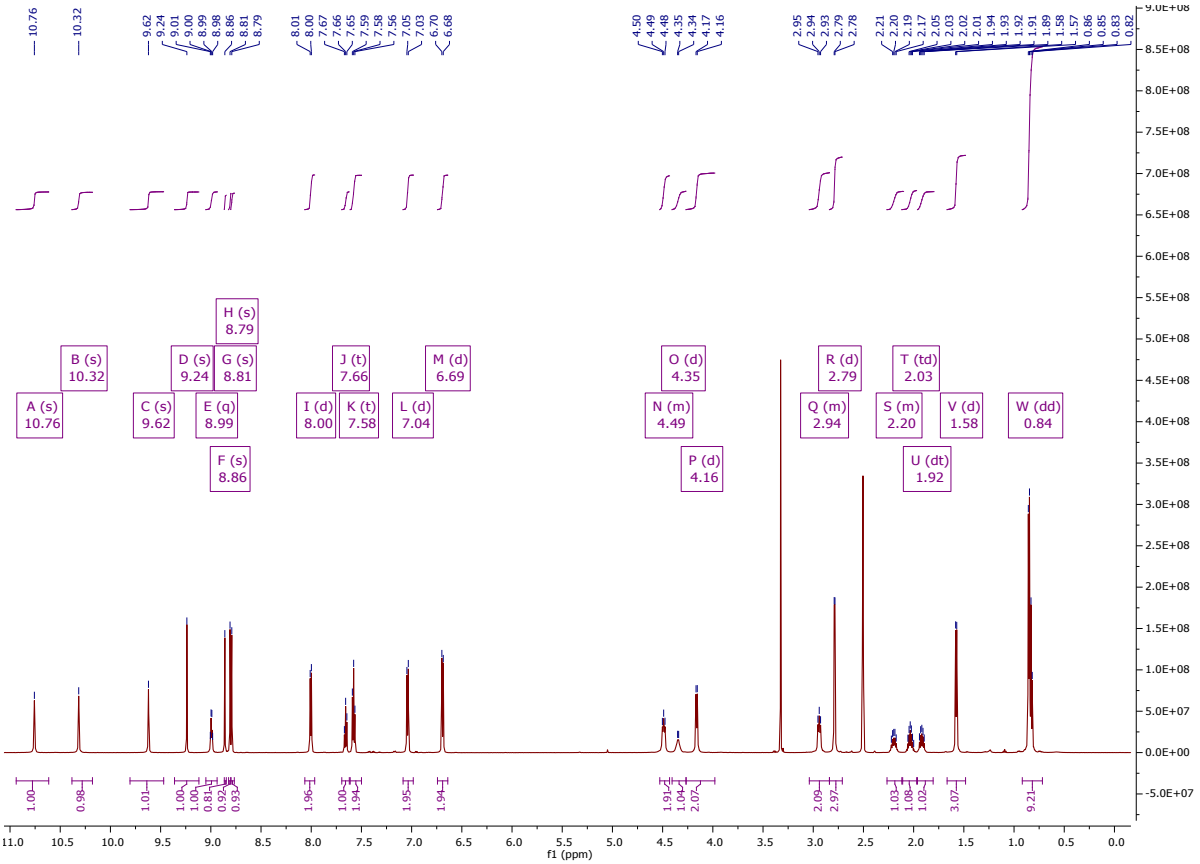

Figure S19. ^{1}H-NMR (600 MHz, DMSO-d_6) of **7b** at room temperature.

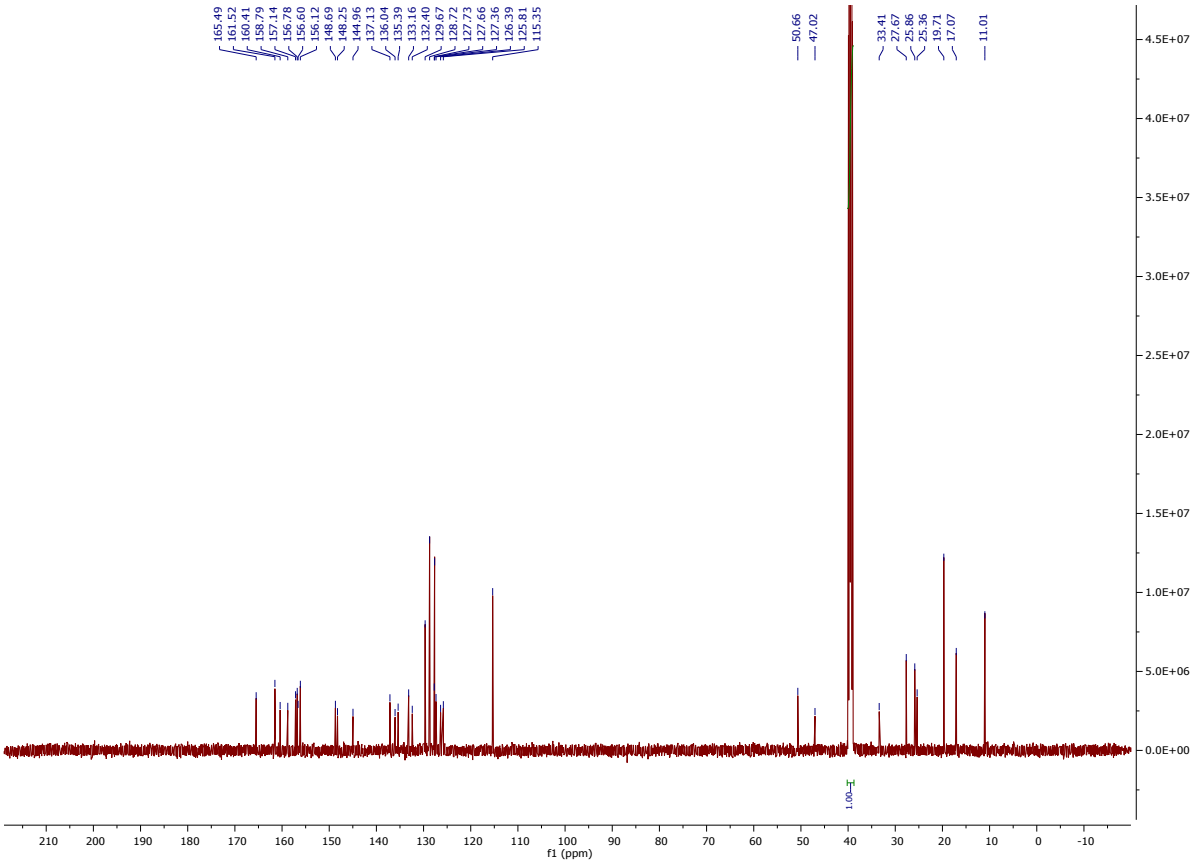

Figure S20. ^{13}C-NMR (151 MHz, DMSO-d_6) of **7b** at room temperature.

2. Saftey Statement

No unusual or unexpected safety related hazards were encountered.

3. Supplementary Figures and Tables

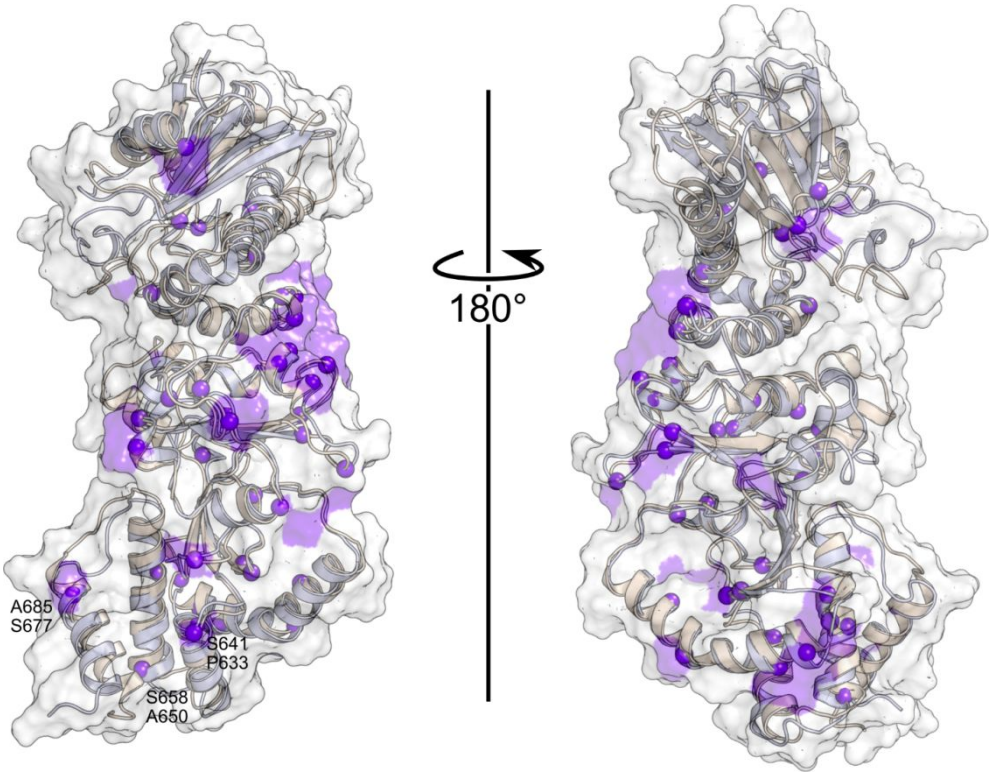

Figure S21: Comparison of Hsp90α and Hsp90β. Overlay of the simulated MD-CTD part of Hsp90α (PDB ID 3q6m) and Hsp90β (PDB ID 5fwk). The isoforms share over 85% sequence identity and are structurally very similar, as shown in the backbone superposition (α: orange; β: blue). Non-identical residues are indicated by purple spheres and labeled in the CTDs' dimerization interface.

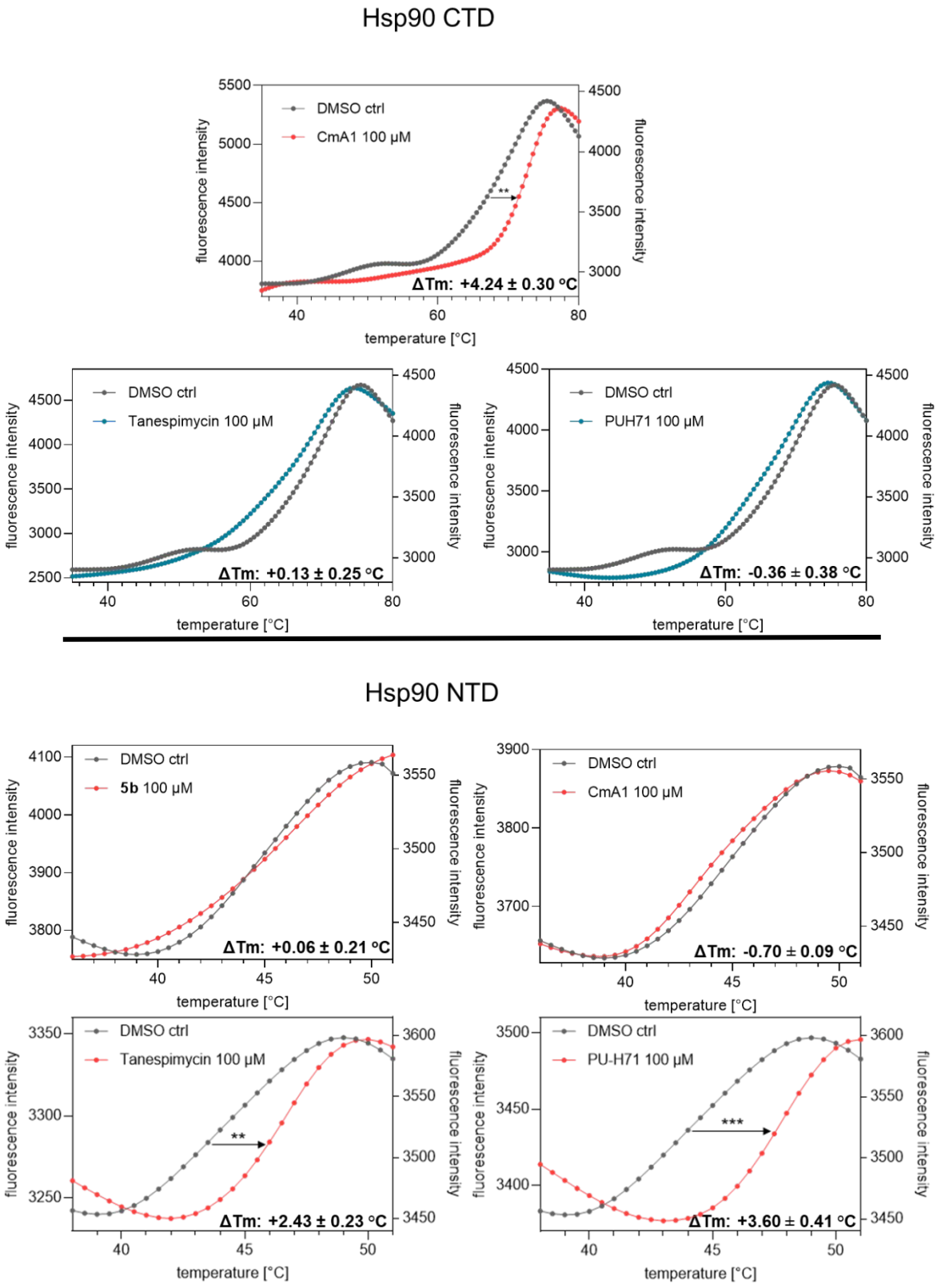

Figure S22: Cell-free thermal shift assay was performed by incubating recombinant Hsp90α CTD (upper panel) and Hsp90α NTD (lower panel) recombinant protein with Coumermycin A1 (CmA1), Tanespimycin, PU-H71 or **5b** (100µM) at increasing temperature (up to 95 °C). Melting temperature (Tm) without inhibitors (DMSO) was used as a control.

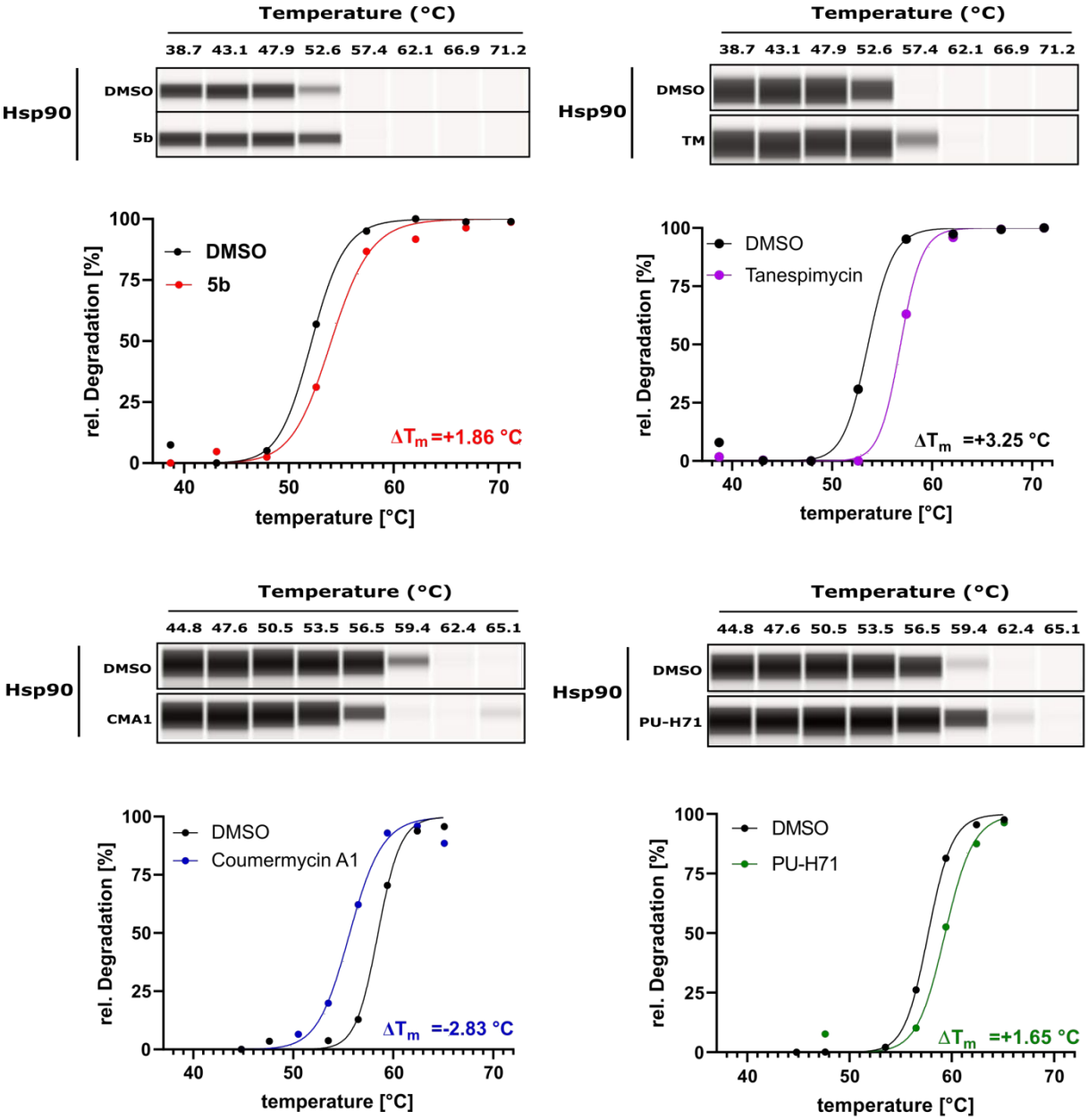

Figure S23: The temperature-dependent intracellular thermal stabilization of t-Hsp90 protein after **5b** incubation with K562 cells for 24 h, at its increasing temperatures. Treated samples were measured by quantitative simple western immunoassay. Protein levels represented by the area under the curve of the electropherograms were normalized to the lowest temperature set as 0% degradation. ΔTm for compounds were determined by plotting normalized data using a sigmoid dose curve and non-linear regression.

Table S1. Comparison of **5b** with the reference Hsp90 CTD and NTD inhibitors in thermal shift assay (Cell-free and cellular), time-resolved fluorescence resonance energy transfer (TR-FRET) assay with labeled PPID (Hsp90-CTD interacting chaperone), fluorescence polarization with FITC-labelled geldanamycin and cell-free recombinant luciferase refolding assay.

Assay	Targeting	Thermal Shift ΔTm [°C] HSP90			TR-FRET HSP90 CTD inhibition %		FP inhibition %	Cell free r-Luciferase refolding Inhibition %
Compound	Domain/Isoform	HSP90α CTD	HSP90α NTD	Cellular	HSP90α	HSP90β	HSP90α NTD	
	[conc.]	[100 µM]	[100 µM]		[1 mM]	[1 mM]	[10 µM]	[100 µM]
5b	Experimental HSP90 CTD	-8.45 ± 0.55	+0.06 ± 0.21	+1.86	92.95 ± 2.96 %	94.76 ± 0.03 %	no inhibition	60%
Coumermycin A1	Reference HSP90 CTD	+4.24 ± 0.30	-0.70 ± 0.09	-2.83	94.99 ± 0.86 %	96.54 ± 0.40 %	20.61 ± 0.44 %	-
Tanespimycin (17-AAG)	Reference HSP90 NTD	+0.13 ± 0.25	+2.43 ± 0.23	+3.25	no Inhibition	57.62 ± 5.53%	90.36 ± 1.39 %	63%
PU-H71	Reference HSP90 NTD	-0.36 ± 0.38	+3.60 ± 0.41	+1.65	no Inhibition	no inhibition	91.23 ± 0.62 %	-

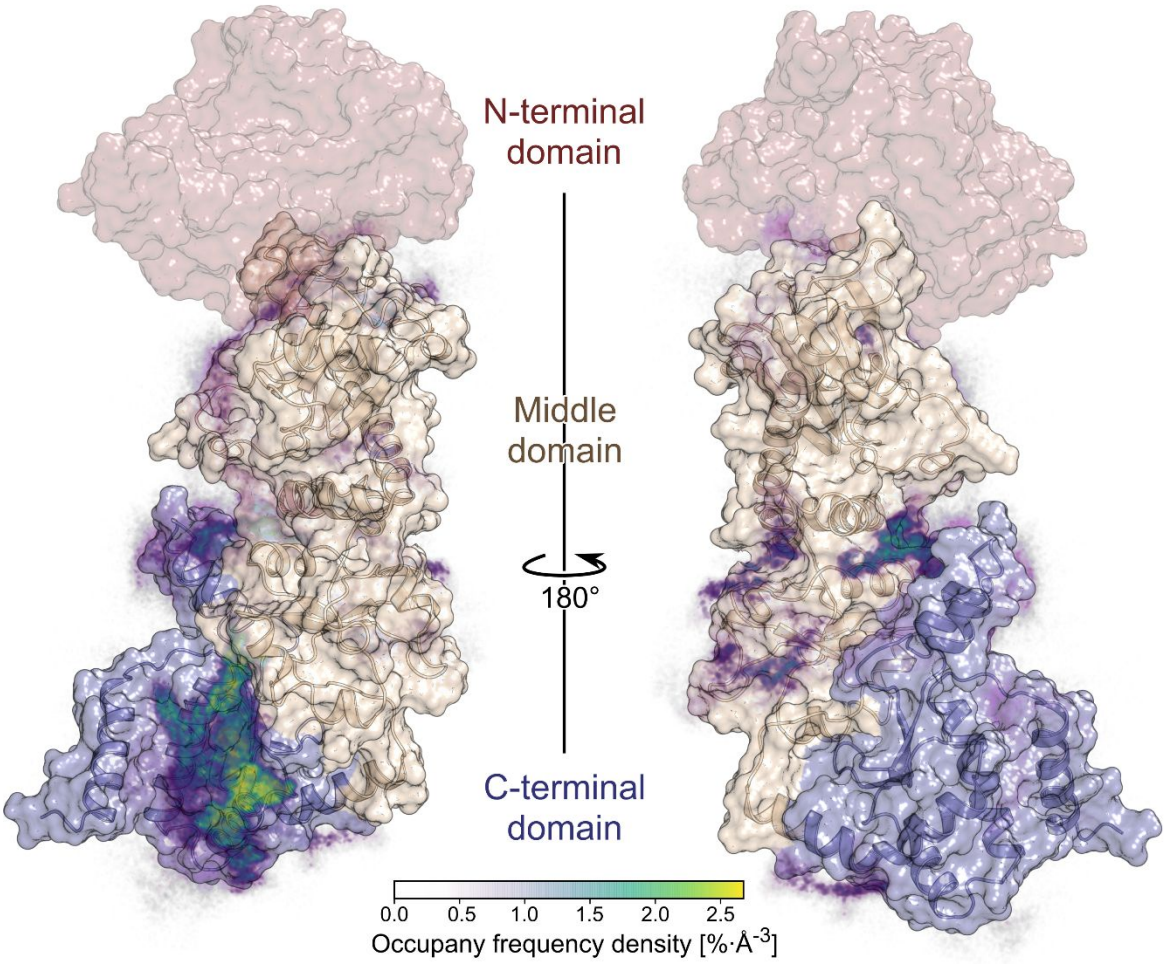

Figure S24: MD simulations of 5b with Hsp90β. The relative densities of the bound poses of **5b** after 500 ns are mapped onto the Hsp90β monomer fragment used in the simulations (PDB ID 5fwk). The missing NTD is shown in red. Particularly high densities are observed in the region between H4 and H5, as in our simulation results for the α isoform (see Fig. 4). The less preferred site in the cleft between the CTD and MD is also observed but with lower density.

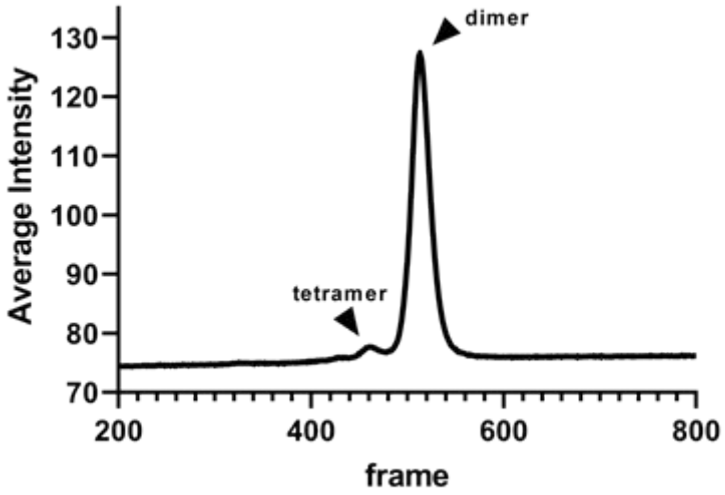

Figure S25: SEC-SAXS elution profile of Hsp90 CTD. Shown is the average intensity of the different frames of the SEC-SAXS elution profile, performed with a Superdex 200 increase 3.2/300 column. The chromatogram was created using CHROMIXS [1]. The arrows indicate the dimer and the tetramer species within the profile. Frames of the corresponding dimer peak and the buffer were merged with CHROMIXS [1].

Table S2. Overall SAXS data of Hsp90α CTD

SAXS Device	**BM29, ESRF Grenoble**[2-3]	**Xenocs Xeuss 2.0 with Q-Xoom**		
Data collection parameters				
Detector	PILATUS 2 M	PILATUS 3 R 300K windowless		
Detector distance (m)	2.827	0.550		
Beam size	200 µm x 200 µm	0.8 mm x 0.8 mm		
Wavelength (nm)	0.099	0.154		
Sample environment	Quartz capillary,1 mm ø	Low Noise Flow Cell, 1 mm ø		
s range (nm^{-1})‡	0.025–6.0	0.10 – 6.0		
Exposure time per frame (s)	2	600		
Sample	**Hsp90 CTD**			
Mode of measurement	SEC-SAXS	batch		
Temperature (°C)	20	20		
Protein concentration (mg/ml)	18	10.8	9.7	9.7
SEC-Column	Superdex 200 increase 3.2/300	-	-	-
Injection volume (µl)	100	50	50	50
Substrate	without	without	LSK82 230 µM	LSK82 1 mM
Structural parameters				
I(0) from *P(r)*	46.78	0.04	0.04	0.05
R_g (real-space from) (nm)	3.29	3.46	3.46	4.11
I(0) from Guinier fit	46.98	0.04	0.04	0.05
s-range for Guinier fit (nm^{-1})	0.170–0.349	0.117–0.350	0.169–0.374	0.216–0.304
R_g (from Guinier fit) (nm)	3.23	3.40	3.46	4.11
points from Guinier fit	19 - 54	4 - 44	14 - 49	24 - 39
D_{max} (nm)	12.21	11.34	11.71	14.83
POROD volume estimate (nm^3)	92.15	103.32	102.28	116.82
Molecular mass (kDa)				
From *I(0)*	46.78	60.93	60.93	70.62
From Qp [4]	55.86	67.08	66.40	79.44
From MoW2 [5]	46.91	58.58	56.80	61.60
From Vc [6]	51.75	62.03	60.67	65.60
Bayesian Inference [7]	49.76	63.86	62.35	74.33
From POROD	56.97	64.58	63.93	73.01
From sequence	42.66 (dimer) 85.32 (tetramer)			
Structure Evaluation				
DAMMIF fit χ^2	1.127	-	-	-
Ambimeter score	0.845	-	-	-
Software				
ATSAS Software Version [8]	3.0.3			
Primary data reduction	CHROMIX [1] / PRIMUS [9]			
Data processing	GNOM [10]			
Ab initio modelling	DAMMIF [11]			
Averaging & superimposing	DAMAVER [12] / SUPCOMB [13]			
Structure evaluation	AMBIMETER [14]			
Model visualization	PyMOL [15]			

‡s = $4\pi\sin(\theta)/\lambda$, 2θ – scattering angle, λ – Xray-wavelength, n.d. not determined

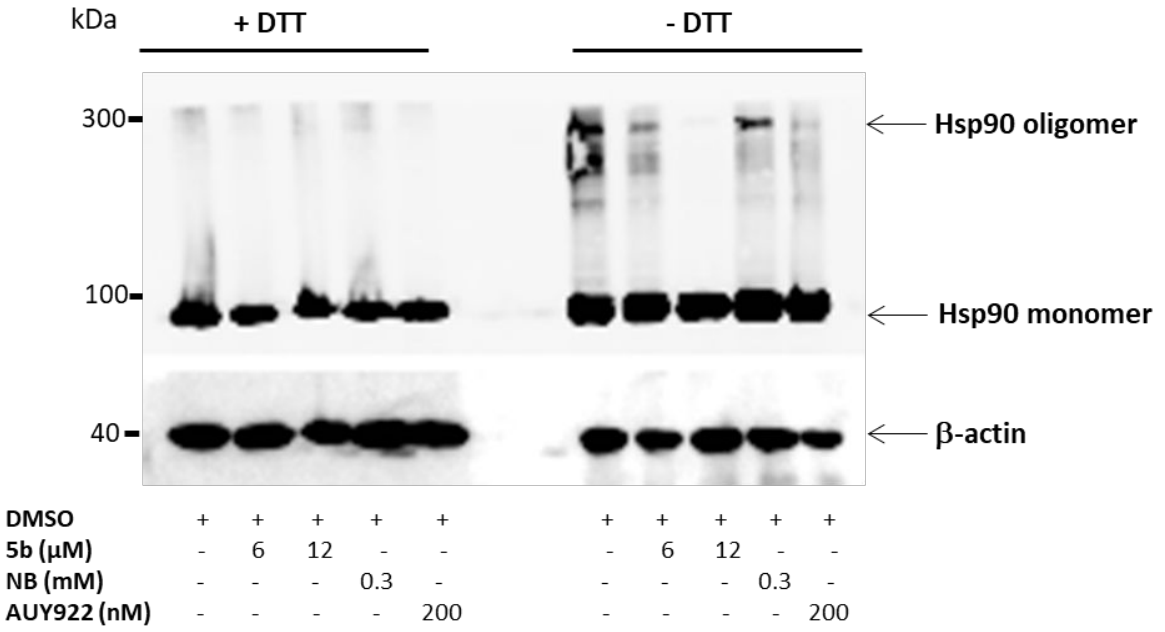

Figure S26: After treating K562 cells with **5b**, NB, or AUY922 for 24 h, lysates were generated with or without reducing conditions (DTT) and were subjected to immunoblot analysis using Hsp90 antibody. An additional oligomeric Hsp90 band appeared in lysates without DTT in control (DMSO), however, the expression of Hsp90 oligomer was abolished after treatment with 5b.

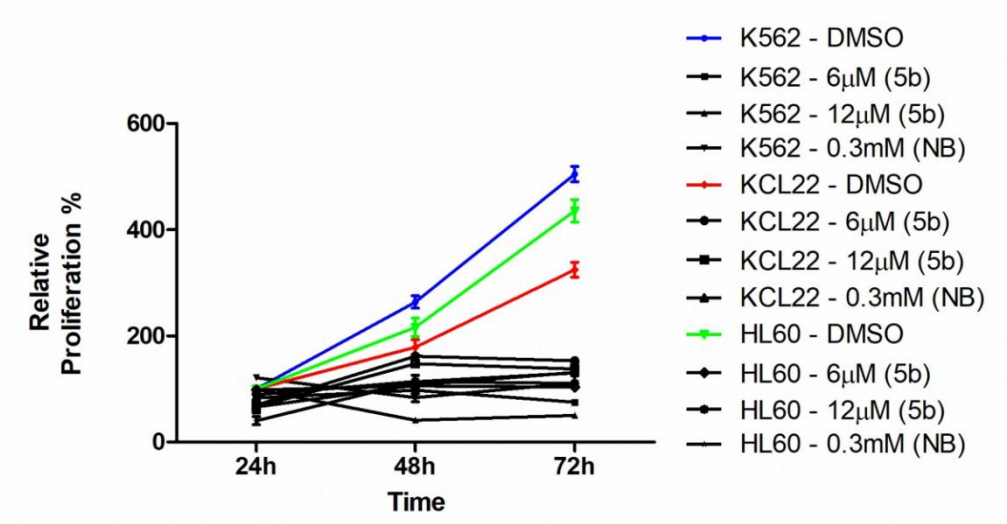

Figure S27. K562, KCL22, and HL60 cell lines were treated with the indicated concentration of **5b** and later viable cells were counted at 24h, 48h, and 72h time periods (n=3).

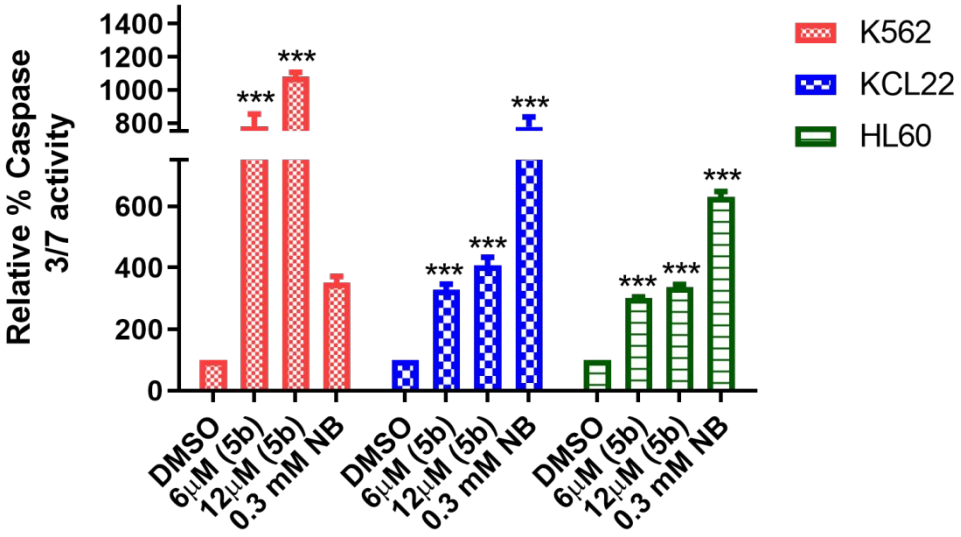

Figure S28. K562, KCL22, and HL60 were treated with **5b** for 48 h. Apoptosis induction was examined using Caspase 3/7 enzyme-dependent glo assay. Columns depict the mean of three independent experiments (n = 3).

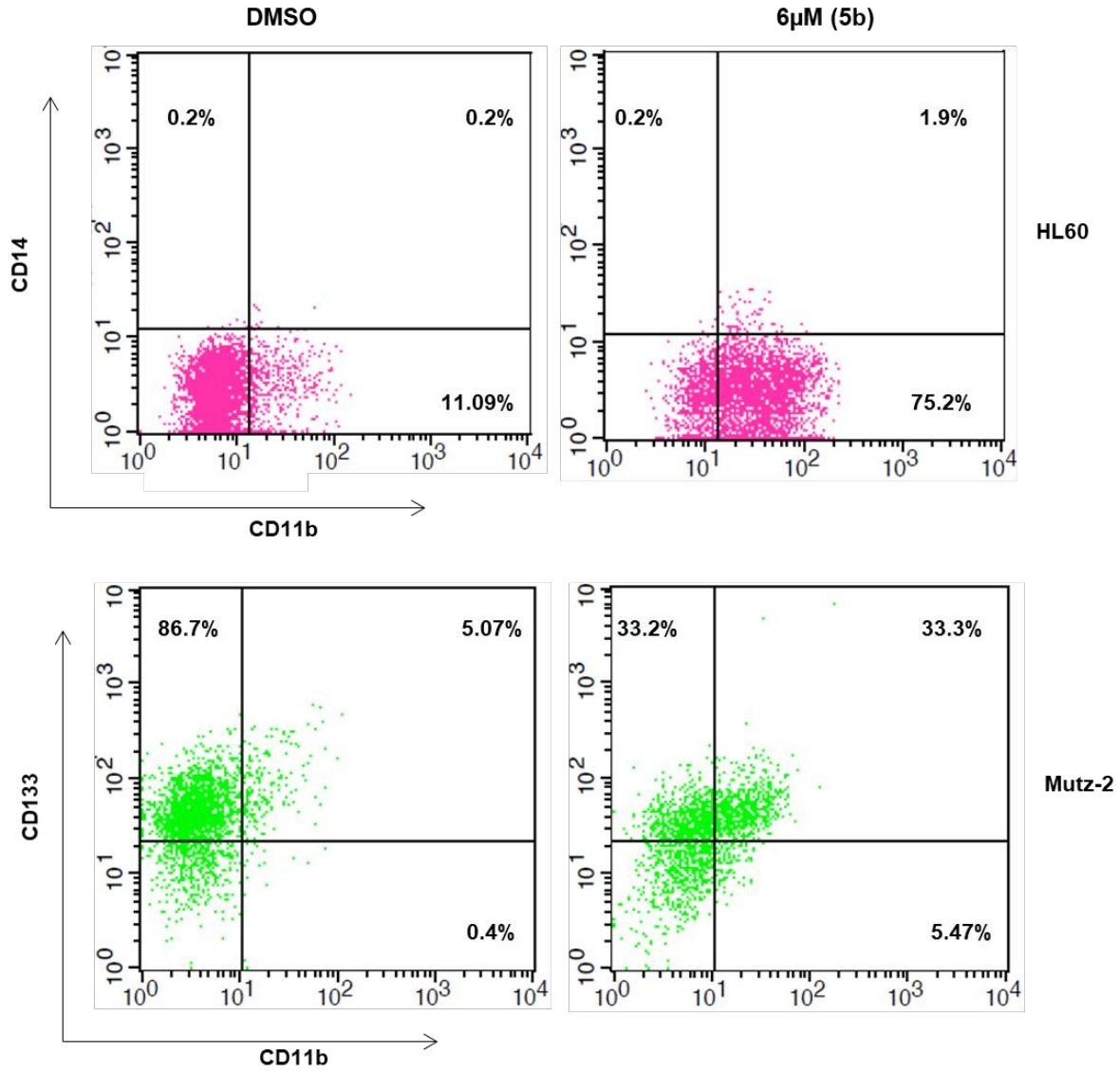

Figure S29. HL60 & Mutz-2 cells were treated with **5b** (6μM) for 48 h and were subjected to FACS after staining with CD11b, CD14 & CD133, CD11b antibodies, respectively. Representative diagram show bivariate FACS analysis of CD14 versus CD11b in HL-60 & CD133 versus CD11b in Mutz-2 cells (n=3).

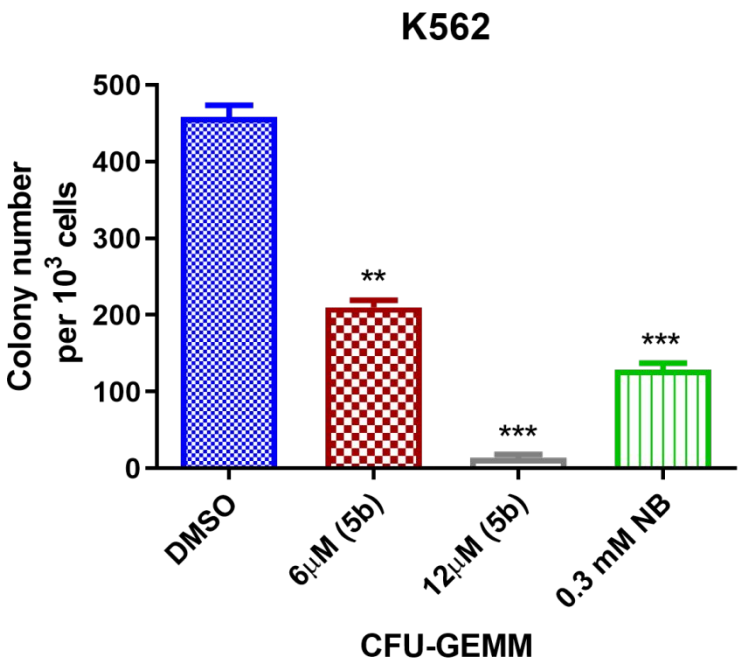

Figure S30. K562 cells were seeded in methylcellulose medium after treatment with **5b** for 24h. Colonies were counted after 14 days. Columns depict the mean of three independent experiments (n = 3).

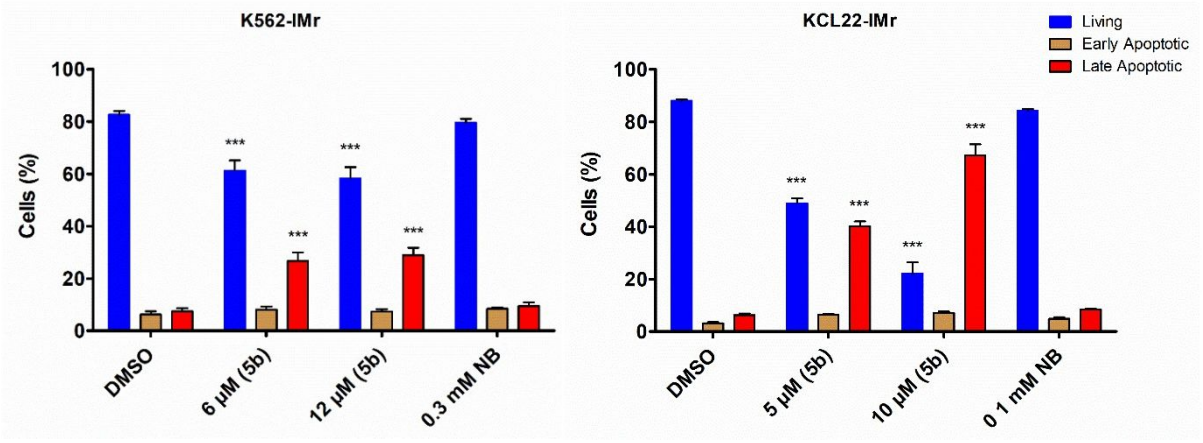

Figure S31. Annexin V/PI staining of K562-IMr and KCL22-IMr after 24 h, 48 h, and 72 h treatment with **5b** and Novobiocin (NB) at indicated doses, based on the determined IC50 determination (n=3). Based on the co-appearance of annexin V/PI staining, the cells were separated in late and early apoptotic stages.

4. Determination of Aqueous Solubility (Thermodynamic Solubility): 5b (or LSK82)

Study Objective

The test articles (**5b** or **LSK82**) and reference compound (Ondansetron) were assessed for thermodynamic solubility in phosphate-buffered saline, pH 7.4.

Materials

1. Reagents and consumables

Phosphate buffered saline, pH 7.4 (Sigma-Aldrich, USA; Cat #P3813)
Acetonitrile Chromasolv, gradient grade, for HPLC, ≥99.9% (Sigma-Aldrich, USA; Cat #34851)
Ondansetron base powder (Enamine, Ukraine, Cat # EN300-117273)
DMSO (Sigma-Aldrich, USA; Cat # 34869)
Costar 96 Well Assay Blocks (Corning, USA; Cat # 3958)
UV-Star® 96 Well Microplate (Greiner Bio-One, Germany; Ca t #655801)
Matrix Disposable pipette tips (ThermoScientific, USA; Cat ## 8041, 7622, 7321)
Flex-Tubes Microcentrifuge Tubes, 1.5ml (Eppendorf, Germany; Cat # 22364111)
MultiScreen HTS 96 Well Filter Plates (Millipore, Ireland; Cat # MSGVS2210)

2. Equipment

Water purification system Millipore Milli-Q Gradient A10 (Millipore, France)
Thermomixer R Block, 1.5 ml (Eppendorf, Germany; Cat # 5355)
Matrix Multichannel Electronic Pipette 2-125 µL, 5-250 µL, 15-1250 µL (Thermo Scientific, USA; Cat ## 2011, 2012, 2004)
SpectraMax Plus Microplate Reader (Molecular Devices, USA; Product # 02196)
Multi-Well Plate Vacuum Manifold (Pall Corporation, USA; Product # 5014)
Vacuum pump (Millipore, USA; Model # XX5500000)

3. Analytical System

The measurements were performed using Spectra Max Plus reader in UV-Vis mode. Acquisition and analysis of the data were performed using SoftMax Pro v.5.4 (Molecular Devices) and Excel 2010 data analysis software.

Methods

The thermodynamic solubility assay was performed according to Enamine's aqueous solubility SOP. Briefly, the dry powder forms of the test compounds were mixed with phosphate-buffered saline pH 7.4 to the theoretical concentration of 4 mM and further allowed to equilibrate at 25°C on a thermostatic shaker. After 4 and 24 hours shaking, incubation mixtures were filtered through HTS filter plates using a vacuum manifold. The filtrates of test compounds were diluted 2-fold with acetonitrile with 4% DMSO before measuring.

In parallel, compounds dilutions in 50% acetonitrile/buffer (pure acetonitrile for **5b** or **LSK82**) were prepared to the theoretical concentrations of 0 µM (blank), 10 µM, 25 µM, 50 µM, 100 µM and 200 µM with 2% final DMSO to generate calibration curves. Ondansetron was used as a reference compound to control proper assay performance. 150 µl of samples was transferred to 96-well plate and measured in 200-550 nm range with 5 nm step.

The concentrations of compounds in PBS are calculated using a dedicated Microsoft Excel calculation script. Proper absorbance wavelengths for calculations are selected for each compound manually based on absorbance maximums (absolute absorbance unit values for the minimum and maximum concentration points within 0 – 3 OD range). Each of the final datasets is additionally visually evaluated by the operator and goodness of fit (R2) is calculated for each calibration curve. The effective range of this assay is approximately 2-400 µM and the compounds returning values close to the upper limit of the range may have higher actual solubility (e.g.5'-deoxy-5-fluorouridine). This method is not suitable for liquid (at 25°C) substances (were not present among the tested compounds).

Results

The solubility data of the test and reference compounds are listed in the table below. The calibration curves are shown in the Appendix. Please note that thermodynamic solubility determined in the conditions of this test depends strongly upon the properties of the solid material used (particular crystal/amorphous form). Hydrophobic, poorly soluble compounds may sometimes have extremely slow kinetics of dissolution resulting in very low solubility values, as opposed to the data from "kinetic solubility" testing, which is usually more relevant for early stages of drug discovery phase.

Table 1. Solubility of compounds in PBS, pH 7.4

Compound ID	**Time Point**	**PBS solubility, pH 7.4, µM**			**SE**
		Incubation 1	**Incubation 2**	**Mean**	
Ondansetron	4h	95	95	95	0.0
	24h	96	93	95	1.6
5b (**LSK82**)	4h	5	5	5	0.0
	24h	7	9	8	1.0

*****Goodness of fit (R2) in all titration curves as well as the variations between repeat measurements indicates high quality of the experimental data in the current batch of the test articles.

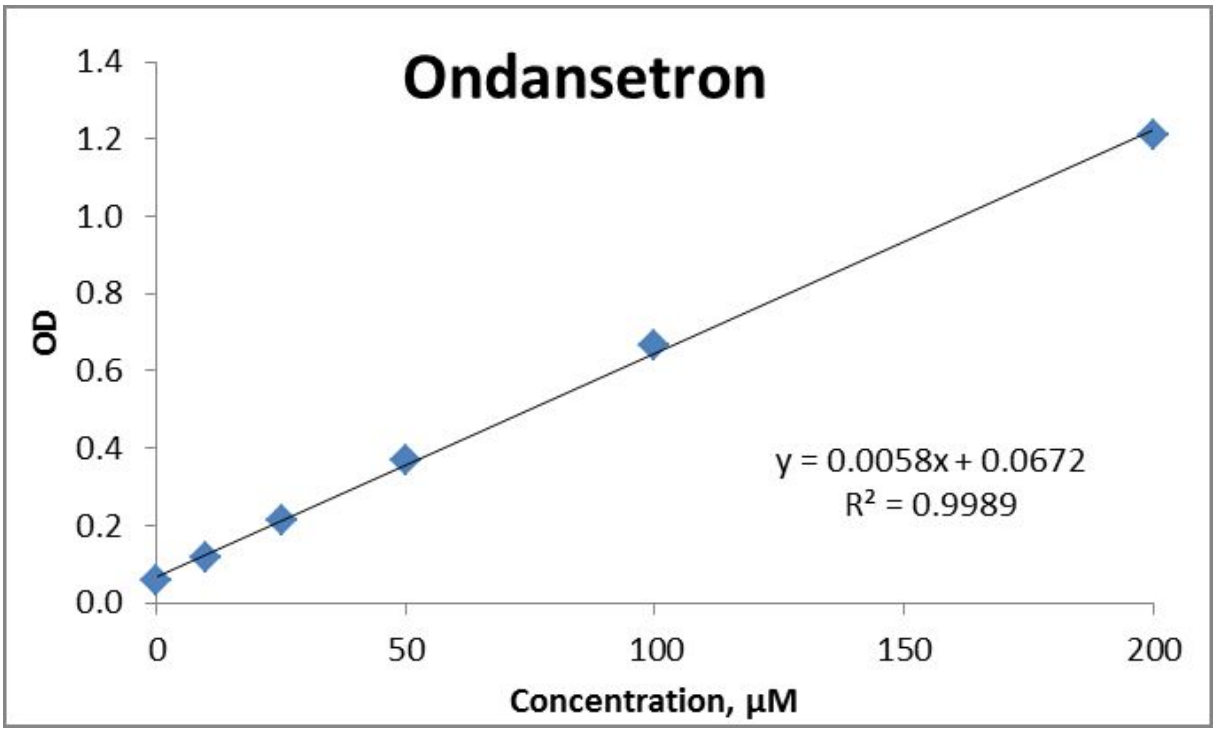

Figure 1. Calibration curve for **Ondansetron**

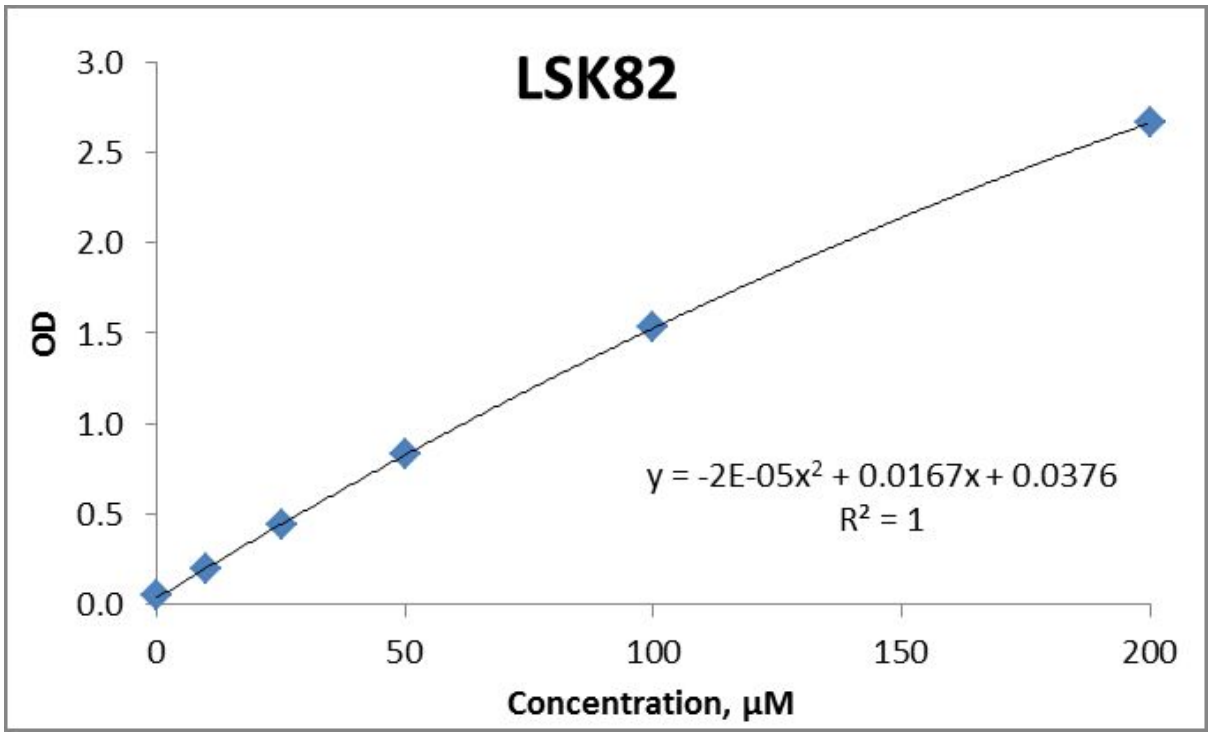

Figure 2. Calibration curve for **5b** (**LSK82**)

4. Assessment of Metabolic Stability in Human Liver Microsomes: 5b (or LSK82)

Study Objective

The objective of this study was to determine metabolic stability of **5b** (**LSK82)** and reference compounds (Propranolol and Diclofenac) in human liver microsomes at five time points over 40 minutes using HPLC-MS. Metabolic stability is defined as the percentage of parent compound lost over time in the presence of a metabolically active test system.

Materials

Reagents and consumables

DMSO (Sigma-Aldrich, 34869 - Chromasolv Plus, for HPLC, ≥99.7%)

Acetonitrile (Sigma-Aldrich, 34851 - Chromasolv Plus, for HPLC, ≥99.9%)

Potassium phosphate monobasic (Helicon, Am-O781-0.5)

Potassium phosphate dibasic (Helicon, Am-O705-0.5)

Magnesium chloride hexahydrate (Helicon, Am-O288-0.1)

Human Liver Microsomes: pooled, mixed gender (XenoTech, H0630/lot N#1810003)

Glucose-6-phosphate dehydrogenase from baker's yeast, type XV (Sigma-Aldrich, G6378)

Glucose-6-phosphate sodium salt (Sigma-Aldrich, G7879)

β-Nicotinamide adeninedinucleotide-2'-phosphate reduced, tetrasodium salt

(Sigma Aldrich N1630-100 MG)

Formic acid (Sigma-Aldrich, 94318)

(+,-) Propranolol hydrochloride (Sigma-Aldrich, P0884)

Diclofenac, 96% purity (Enamine, # EN300-119509)

Phenomenex Luna® C18 HPLC column, 2.1x50 mm, 5 µm (Cat #5291-126)

1.1 ml microtubes in microracks, pipettor tips (Thermo Scientific).

Equipment

Gradient HPLC system (Shimadzu)

Triple quadrapole mass-detector API 3000 with TurboIonSpray Ion Source (AB Sciex, Canada)

Nitrogen generator N2-04-L1466, nitrogen purity 99%+ (Whatman)

Environmental Incubator Shaker G24; Digital Refrigerated Incubator/Shaker Innova 4330 (New Brunswick Scientific)

Water purification system Millipore Milli-Q Gradient A10 (Millipore, France)

Multichannel pipettors 5-250 µL, 2-125 µL, 15-1250 µL (Thermo Scientific)

Analytical System

All measurements were performed using Shimadzu Prominence HPLC system including vacuum degasser, gradient pumps, reverse phase column, column oven and autosampler. The HPLC system was coupled with tandem mass spectrometer API 3000 (PE Sciex). The both positive and negative ion modes of the TurboIonSpray ion source were used. Acquisition and analysis of the data were performed using Analyst 1.5.2 software (PE Sciex).

Methods

Microsomal incubations were carried out in 96-well plates in 5 aliquots of 40 µL each (one for each time point). Liver microsomal incubation medium comprised of phosphate buffer (100 mM, pH 7.4), MgCl2 (3.3 mM), NADPH (3 mM), glucose-6-phosphate (5.3 mM), glucose-6-phosphate dehydrogenase (0.64 units/ml) with 0.42 mg of liver microsomal protein per ml. In the control reactions the NADPH-cofactor system was substituted with phosphate buffer. Test compounds (2 µM, final solvent concentration 1.6 %) were incubated with microsomes at 37 ˚C, shaking at 100 rpm. Each reaction was performed in duplicates. Five time points over 40 minutes were analyzed. The reactions were stopped by adding 5 volumes of 90% acetonitrile-water to incubation aliquots, followed by protein sedimentation by centrifuging at 5500 rpm for 3 minutes. Each reaction was performed in duplicates. Supernatants were analyzed using the HPLC system coupled with tandem mass spectrometer. The elimination constant

(kel), half-life (t1/2) and intrinsic clearance (Clint) were determined in plot of ln(AUC) versus time, using linear regression analysis:[16]

$$k_{el} = -slope$$

$$t_{1/2} = \frac{0.693}{k}$$

$$Cl_{\text{int}} = \frac{0.693}{t_{1/2}} \times \frac{\mu l_{incubation}}{mg_{microsomes}}$$

In order to indicate the quality of the linear regression analysis, the R (correlation coefficient) values are provided. In some cases, the last time point is excluded from the calculations to ensure acceptable logarithmic linearity of decay.[16]

Results

Human microsomal stability data for reference and test compounds is provided in the table below.

Table 1. Human microsomal stability

Compound ID	Time, min	Analyte Peak Area		Analyte Peak Area, Mean of 2	% Remaining, Mean of 2	R	kel, min-1	$t_{1/2}$, min	C_{lint}, µl/min/mg	% Remaining without cofactor, Mean of 2
		Inc. 1	Inc. 2							
1	2	3	4	5	6	7	8	9	10	11
Propranolol human	0	9.98E+04	9.84E+04	9.91E+04	100	0.947	0.008	82.5	20	100
	7	9.73E+04	9.80E+04	9.77E+04	99	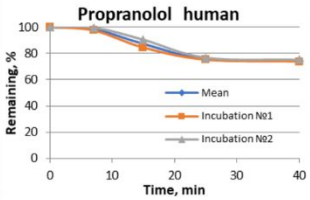				
	15	8.42E+04	8.89E+04	8.66E+04	87					
	25	7.50E+04	7.55E+04	7.53E+04	76					
	40	7.36E+04	7.40E+04	7.38E+04	74					103
Diclofenac human	0	2.24E+05	2.09E+05	2.17E+05	100	0.991	0.096	7.2	231	100
	7	1.65E+05	1.66E+05	1.66E+05	76	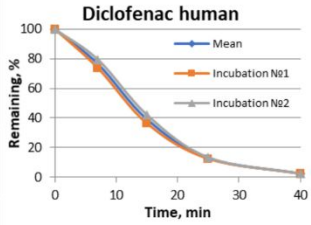				
	15	8.10E+04	8.79E+04	8.45E+04	39					
	25	2.78E+04	2.80E+04	2.79E+04	13					
	40	5.27E+03	5.34E+03	5.31E+03	2					95
5b (LSK82)	0	8.48E+04	8.48E+04	8.48E+04	100	0.894*	0.003*	261.2*	6*	100
	7	8.22E+04	8.24E+04	8.23E+04	97	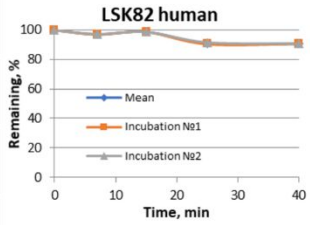				
	15	8.37E+04	8.37E+04	8.37E+04	99					
	25	7.67E+04	7.75E+04	7.71E+04	91					
	40	7.68E+04	7.68E+04	7.68E+04	91					96

*Parameter should be considered as approximate due to the high stability of the compound

Interpretation of microsomal stability assay data

The test compounds can be classified in terms of their microsomal stability into low, medium and high clearance groups. The intrinsic clearance classification bands for mouse, rat, and human species are calculated according to the well stirred model equation:[16]

$$CL_{int} = \frac{CLH}{fu\ x\ (1-E)}$$

where CLH is a hepatic clearance (mL/min/kg), CLH = E x QH
QH = liver blood flow (mL/min/kg)[17]
E = extraction ratio, assumed at 0.3 for low clearance and at 0.7 for high clearance compounds
fu = fraction unbound in plasma, assumed at 1.

The CLint classification values were calculated for mouse, rat, and human species using the literature data on liver weight[3] and microsomal protein concentration[18-19] and are represented in the following table.

The intrinsic clearance groups for classification of test compounds

Classification group	Intrinsic clearance (μL/min/mg protein)		
	Mouse	Rat	Human
Low clearance	<8.6	<13	<8.8
High clearance	>48	>72	>48

5. Supplementary References

1. Panjkovich, A.; Svergun, D. I., CHROMIXS: automatic and interactive analysis of chromatography-coupled small angle X-ray scattering data. *Bioinformatics* **2017**.
2. Pernot, P.; Round, A.; Barrett, R.; De Maria Antolinos, A.; Gobbo, A.; Gordon, E.; Huet, J.; Kieffer, J.; Lentini, M.; Mattenet, M.; Morawe, C.; Mueller-Dieckmann, C.; Ohlsson, S.; Schmid, W.; Surr, J.; Theveneau, P.; Zerrad, L.; McSweeney, S., Upgraded ESRF BM29 beamline for SAXS on macromolecules in solution. *J Synchrotron Radiat* **2013,** *20* (Pt 4), 660-4.
3. Pernot, P.; Theveneau, P.; Giraud, T.; Fernandes, R. N.; Nurizzo, D.; Spruce, D.; Surr, J.; McSweeney, S.; Round, A.; Felisaz, F.; Foedinger, L.; Gobbo, A.; Huet, J.; Villard, C.; Cipriani, F., New beamline dedicated to solution scattering from biological macromolecules at the ESRF. *Journal of Physics: Conference Series* **2010,** *247* (1), 012009.
4. Porod, G., Die Röntgenkleinwinkelstreuung Von Dichtgepackten Kolloiden Systemen - 1 Teil. *Kolloid Z Z Polym* **1951,** *124* (2), 83-114.
5. Fischer, H.; Neto, M. D.; Napolitano, H. B.; Polikarpov, I.; Craievich, A. F., Determination of the molecular weight of proteins in solution from a single small-angle X-ray scattering measurement on a relative scale. *J Appl Crystallogr* **2010,** *43*, 101-109.
6. Rambo, R. P.; Tainer, J. A., Accurate assessment of mass, models and resolution by small-angle scattering. *Nature* **2013,** *496* (7446), 477-81.
7. Hajizadeh, N. R.; Franke, D.; Jeffries, C. M.; Svergun, D. I., Consensus Bayesian assessment of protein molecular mass from solution X-ray scattering data. *Sci Rep* **2018,** *8* (1), 7204.
8. Manalastas-Cantos, K.; Konarev, P. V.; Hajizadeh, N. R.; Kikhney, A. G.; Petoukhov, M. V.; Molodenskiy, D. S.; Panjkovich, A.; Mertens, H. D. T.; Gruzinov, A.; Borges, C.; Jeffries, C. M.; Svergun, D. I.; Franke, D., ATSAS 3.0: expanded functionality and new tools for small-angle scattering data analysis. *J Appl Crystallogr* **2021,** *54* (1).
9. Konarev, P. V.; Volkov, V. V.; Sokolova, A. V.; Koch, M. H. J.; Svergun, D. I., PRIMUS: a Windows PC-based system for small-angle scattering data analysis. *J Appl Crystallogr* **2003,** *36*, 1277-1282.
10. Svergun, D. I., Determination of the Regularization Parameter in Indirect-Transform Methods Using Perceptual Criteria. *J Appl Crystallogr* **1992,** *25*, 495-503.
11. Franke, D.; Svergun, D. I., DAMMIF, a program for rapid ab-initio shape determination in small-angle scattering. *J Appl Crystallogr* **2009,** *42*, 342-346.
12. Volkov, V. V.; Svergun, D. I., Uniqueness of ab initio shape determination in small-angle scattering. *J Appl Crystallogr* **2003,** *36* (3 Part 1), 860-864.
13. Kozin, M. B.; Svergun, D. I., Automated matching of high- and low-resolution structural models. *J Appl Crystallogr* **2001,** *34*, 33-41.
14. Petoukhov, M. V.; Svergun, D. I., Ambiguity assessment of small-angle scattering curves from monodisperse systems. *Acta Crystallogr D Biol Crystallogr* **2015,** *71* (Pt 5), 1051-8.
15. PyMOL, The PyMOL Molecular Graphics System, Version 2.0 Schrödinger, LLC. **2015**.
16. Houston, J. B., Utility of in vitro drug metabolism data in predicting in vivo metabolic clearance. *Biochem Pharmacol* **1994,** *47* (9), 1469-79.
17. Davies, B.; Morris, T., Physiological parameters in laboratory animals and humans. *Pharm Res* **1993,** *10* (7), 1093-5.
18. Barter, Z. E.; Bayliss, M. K.; Beaune, P. H.; Boobis, A. R.; Carlile, D. J.; Edwards, R. J.; Houston, J. B.; Lake, B. G.; Lipscomb, J. C.; Pelkonen, O. R.; Tucker, G. T.; Rostami-Hodjegan, A., Scaling factors for the extrapolation of in vivo metabolic drug clearance from in vitro data: reaching a consensus on values of human microsomal protein and hepatocellularity per gram of liver. *Curr Drug Metab* **2007,** *8* (1), 33-45.
19. Iwatsubo, T.; Suzuki, H.; Sugiyama, Y., Prediction of species differences (rats, dogs, humans) in the in vivo metabolic clearance of YM796 by the liver from in vitro data. *J Pharmacol Exp Ther* **1997,** *283* (2), 462-9.